



Published in final edited form as:

Nat Cell Biol. 2022 February ; 24(2): 181–193. doi:10.1038/s41556-021-00840-5.

LONP-1 and ATFS-1 sustain deleterious heteroplasmy by promoting mtDNA replication in dysfunctional mitochondria

Qiyuan Yang¹, Pengpeng Liu¹, Nadine S. Anderson¹, Tomer Shpilka¹, YunGuang Du¹, Nandhitha Uma Naresh¹, Rui Li¹, Lihua Julie Zhu¹, Kevin Luk¹, Josh Lavelle¹, Rilee D. Zeinert^{2,3}, Peter Chien^{2,3}, Scot A. Wolfe¹, Cole M. Haynes^{1,*}

¹Department of Molecular, Cell and Cancer Biology, UMass Chan Medical School, Worcester, MA 01605, USA.

²Department of Biochemistry and Molecular Biology, University of Massachusetts Amherst, MA 01002, USA

³Molecular and Cellular Biology Graduate Program, University of Massachusetts Amherst, MA 01002, USA

Abstract

The accumulation of deleterious mitochondrial DNA (mtDNA) causes inherited mitochondrial diseases and aging-associated decline in mitochondrial functions such as oxidative phosphorylation (OXPHOS) function. Upon mitochondrial perturbations, the bZIP protein ATFS-1 induces a transcription program to restore mitochondrial function. Paradoxically, ATFS-1 is also required to maintain mtDNAs in heteroplasmic worms. The mechanism(s) by which ATFS-1 promotes mtDNA accumulation relative to wildtype mtDNAs is unclear. Here, we show that ATFS-1 accumulates in dysfunctional mitochondria. ATFS-1 is absent in healthy mitochondria due to degradation by the mtDNA-bound protease LONP-1, resulting in the nearly exclusive association between ATFS-1 and mtDNAs in heteroplasmic worms. Moreover, we demonstrate that mitochondrial ATFS-1 promotes the binding of the mtDNA replicative polymerase (POLG) to mtDNAs. Interestingly, inhibition of the mtDNA-bound protease LONP-1 increased ATFS-1 and POLG binding to wildtype mtDNAs. LONP-1 inhibition in *C. elegans* and human cybrid cells improved the heteroplasmy ratio and restored OXPHOS. Our findings suggest that ATFS-1 promotes mtDNA replication in dysfunctional mitochondria by promoting POLG-mtDNA binding, which is antagonized by LONP-1.

Users may view, print, copy, and download text and data-mine the content in such documents, for the purposes of academic research, subject always to the full Conditions of use: <https://www.springernature.com/gp/open-research/policies/accepted-manuscript-terms>

*Lead Contact: Correspondence to: cole.haynes@umassmed.edu.

AUTHOR CONTRIBUTIONS

Q.Y. and C.M.H. planned the experiments. Q.Y., Y.D., T.S., N.N., J.L., R.Z. and P.C. generated the worm strains. R.L. and L.J.Z. analyzed ATFS-1::GFP and TMRE quantification. Q.Y. performed the *C. elegans* and cybrid mtDNA analysis including ChIP and respiratory function. P.L., K.L. and S.W. performed and analyzed mtDNA sequencing. Q.Y., N.S.A. and C.M.H. wrote the manuscript.

Competing Interests Statement

The authors declare no competing interests.

Keywords

ATFS-1; LONP-1; heteroplasmy; mitochondrial DNA (mtDNA)

INTRODUCTION

Mitochondria provide numerous metabolic functions including being the site of energy production via oxidative phosphorylation (OXPHOS). Most of the ~1200 proteins comprising the mitochondrial proteome are encoded by nuclear genes and are imported into each mitochondrion following synthesis on cytosolic ribosomes¹. However, 13 essential OXPHOS components alongside the tRNAs and rRNAs required for their synthesis are encoded by mitochondrial genomes (mtDNAs), which reside in the mitochondrial matrix. Each mitochondrion harbors at least one mtDNA, and most cells harbor 100s-1,000s of mtDNAs.

Mitochondrial function declines as cells age which is accelerated in multiple diseases including Parkinson's Disease. A variety of mitochondrial diseases are caused by inherited mutations that impair OXPHOS function. The disease causing mutations can occur in genes required for OXPHOS encoded by either the nuclear genome, or mtDNAs, which acquire mutations at a significantly higher rate². Single nucleotide variants and deletions are associated with inherited mitochondrial diseases affecting ~1:4000 individuals³. Because of the high number of mtDNAs per cell, a single mutant mtDNA has little impact. To cause the OXPHOS dysfunction that underlies mitochondrial diseases, the mutant mtDNA must accumulate to ~60% of the total cellular mtDNAs. The mixture of mutant mtDNAs and wildtype mtDNAs is known as heteroplasmy. Studies using mitochondrial-targeted nucleases that specifically cleave mutant mtDNAs suggest that a relatively modest reduction in the percentage of mtDNAs is sufficient to improve mitochondrial function^{4,5}.

The initial mtDNA mutation or deletion likely occurs because of an error in mtDNA replication⁶. Two mechanisms are thought to contribute to the "clonal expansion" of the mtDNA. In dividing cells, non-selective genetic drift can disproportionately increase either genome. An alternative model suggests that large mtDNA deletions allow for quicker replication simply because these genomes are smaller^{6,7}. Consistent with both models, inhibition of the replicative mtDNA polymerase POLG causes preferential depletion of mutant mtDNAs^{8,9}. However, the underlying mechanism(s) that confer a replicative advantage and drive the clonal amplification of mtDNAs to a high enough percentage to cause OXPHOS defects in mitochondrial diseases¹⁰⁻¹³, aging¹⁴ and Parkinson's Disease¹⁵ remain unresolved.

Previously, the bZIP protein ATFS-1 was found to be required to maintain deleterious heteroplasmy in *C. elegans*^{9,16}. ATFS-1 harbors both a mitochondrial targeting sequence (MTS) and a nuclear localization sequence (NLS) (Fig. 1a) and regulates a transcriptional program known as the mitochondrial unfolded protein response (UPR^{mt})¹⁷. Under basal conditions, the majority of ATFS-1 is imported into mitochondria, where it is degraded by the protease LONP-1. Mitochondrial dysfunction reduces mitochondrial import capacity, resulting in a percentage of ATFS-1 trafficking to the nucleus, where it activates a

transcriptional program to recover mitochondrial function¹⁸. Importantly, both nuclear and mitochondrial accumulation of ATFS-1 are required for development during mitochondrial dysfunction^{9, 17}. However, the function of ATFS-1 within mitochondria is unclear.

Here, we report that the maintenance of deleterious heteroplasmy requires the accumulation of ATFS-1 within dysfunctional mitochondria. In a heteroplasmic *C. elegans* strain, ATFS-1 binds predominantly to mtDNAs. Moreover, the replicative polymerase POLG also binds predominantly to mtDNAs. Lastly, we demonstrate that the mitochondrial protease LONP-1, which degrades ATFS-1 in functional mitochondria^{17, 19}, is required to establish the enriched interaction between mtDNAs, ATFS-1 and POLG in heteroplasmic worms. Our findings in *C. elegans* are conserved in cultured human cells as inhibition of LONP1 by siRNA or the drug CDDO²⁰, improves heteroplasmy and rescues OXPHOS function in heteroplasmic cells.

RESULTS

OXPHOS perturbations increase mtDNA quantity

OXPHOS proteins are encoded by genes located within the mitochondria and the nucleus. The heteroplasmic *C. elegans* strain *uaDf5* harbors approximately 40% wildtype mtDNAs and 60% mtDNAs that lack four essential OXPHOS protein coding genes (Fig. 1b)²¹. *uaDf5* worms have impaired respiration⁹, constitutive UPR^{mt} activation, as determined by increased expression of the *hsp-6_{pr}::gfp* reporter^{9, 16} (Fig. 1c), and increased total mtDNAs (Fig. 1d)²¹.

To examine the impact of OXPHOS perturbation on mtDNA content, we impaired several OXPHOS components in wildtype homoplasmic worms. As expected, worms raised on *cco-1*(RNAi) (complex IV) or *cyc-1*(RNAi) (cytochrome c) had increased *hsp-6_{pr}::gfp* activation, as did *isp-1(qm150)* (complex III) or *clk-1(qm30)* (ubiquinone biosynthesis) mutant strains (Fig. 1e,f). Intriguingly, each of the OXPHOS perturbations resulted in increased mtDNA content as determined by qPCR (Fig. 1g,h and Extended Data Fig. 1a), which is consistent with previous reports^{22, 23}. Importantly, the increase in mtDNAs caused by OXPHOS perturbation was impaired in *atfs-1(null)* worms that lack the entire *atfs-1* open reading frame²⁴ (Fig. 1g) as well as in worms raised on *atfs-1*(RNAi) (Fig. 1h). Similarly, total mtDNAs in heteroplasmic worms was also reduced when raised on *atfs-1*(RNAi) (Fig. 1d). Combined, these findings indicate that the increased mtDNA content in both homoplasmic and heteroplasmic worms caused by OXPHOS perturbation requires *atfs-1*.

POLG-mtDNA binding during OXPHOS dysfunction requires ATFS-1

We next sought to gain insight into the mechanism by which mtDNAs are increased during OXPHOS perturbation. We previously found that ATFS-1 accumulates within mitochondria when mitochondrial function is perturbed by inhibiting the mitochondrial protease SPG-7 or by raising worms in the presence of ethidium bromide, which impairs mtDNA replication^{17, 19}. Intriguingly, ChIP-sequencing indicated that ATFS-1 binds mtDNAs during mitochondrial dysfunction within the non-coding region (NCR)¹⁷, which in mammals contains sequence elements that regulate mtDNA replication²⁵. Here, we found that ATFS-1

also accumulates in the mitochondrial fraction of worms raised on *cco-1*(RNAi) (Fig. 2a). Furthermore, ATFS-1::GFP also accumulates within mitochondria raised on *cco-1*(RNAi), while TMRE staining was decreased (Fig. 2b) indicative of impaired OXPHOS. Lastly, ATFS-1 ChIP followed by qPCR indicated that ATFS-1 interacts with mtDNA when worms are raised on *cco-1*(RNAi) (Fig. 2c). Combined these data indicate that ATFS-1 accumulates within mitochondria and interacts with mtDNAs when OXPHOS is impaired.

To further explore the relationship between ATFS-1 accumulation and the mtDNA increase during OXPHOS perturbation, we generated POLG antibodies which detected a ~120 KD band that co-fractionated with the OXPHOS protein NDUFS3 (Extended Data Fig. 1b) and was depleted by *polg*(RNAi) (Extended Data Fig. 1c). Similar to ATFS-1, POLG protein levels increased when raised on *cco-1*(RNAi) (Fig. 2d), and POLG interacted with more mtDNAs (Fig. 2e). To determine if the increased POLG-mtDNA interaction required ATFS-1, we performed POLG ChIP-mtDNA in wildtype and *atfs-1*(null) worms raised on *cco-1*(RNAi). Interestingly, the increased POLG-mtDNA interaction was impaired in *atfs-1*(null) worms, suggesting that ATFS-1 is required for increased POLG-mtDNA binding during OXPHOS dysfunction (Fig. 2e).

As *atfs-1* is required for the increase in *polg* mRNA during mitochondrial dysfunction^{9, 19}, we sought to determine if the increased POLG-mtDNA binding required nuclear-localized ATFS-1. We previously generated the *atfs-1^{nuc(-)}* strain in which the NLS within ATFS-1 was impaired via genome editing (Extended Data Fig. 2a,b)¹⁸. Importantly, the *atfs-1^{nuc(-)}* allele impaired *hsp-6* mRNA accumulation when raised on *spg-7*(RNAi) (Extended Data Fig. 2c). Furthermore, the *atfs-1^{nuc(-)}* mutation also impaired *hsp-6_{pr::gfp}* induction in *atfs-1(et18)* worms, which constitutively activates UPR^{mt} due to a mutation that reduces its import into mitochondria^{18, 26} (Extended Data Fig. 2d-f). Induction of *hsp-6* and *polg* mRNA was also impaired in *atfs-1^{nuc(-)}* worms when raised on *cco-1*(RNAi) (Extended Data Fig. 2g,h). Unlike in wildtype worms, POLG protein was not increased in *atfs-1^{nuc(-)}* worms indicating that *atfs-1^{nuc(-)}* worms were unable to regulate nuclear transcription during OXPHOS perturbation (Extended Data Fig. 2h,i). Importantly, ATFS-1^{nuc(-)} accumulated within mitochondria similarly to wildtype ATFS-1 upon LONP-1 inhibition (Extended Data Fig. 2j) indicating the protein was expressed and processed similarly to wildtype ATFS-1. Lastly, ATFS-1^{nuc(-)} bound similar amounts of mtDNA as wildtype ATFS-1 when raised on *cco-1*(RNAi) as determined by ChIP (Fig. 2c,f).

To determine if the nuclear function of ATFS-1 is required for POLG to bind mtDNAs during OXPHOS perturbation, we examined the POLG-mtDNA interaction in *atfs-1*(null) and *atfs-1^{nuc(-)}* worms raised on control or *cco-1*(RNAi). Strikingly, significantly more POLG was bound to mtDNA in *atfs-1^{nuc(-)}* worms relative to *atfs-1*(null) worms (Fig. 2g), suggesting that the *atfs-1*-dependent increase in POLG-mtDNA binding during OXPHOS perturbation does not require the nuclear activity of ATFS-1. mtDNA content also increased in *atfs-1^{nuc(-)}* worms upon OXPHOS perturbation caused by *cco-1*(RNAi) (Fig. 2h) as well as in *clk-1(qm30)* worms (Fig. 2i). Combined, these results suggest that the accumulation of ATFS-1 within mitochondria during OXPHOS perturbation is required to increase POLG-mtDNA binding and mtDNA content.

ATFS-1 degradation by LONP-1 impairs mtDNA propagation

We next sought to determine the events leading to the accumulation of ATFS-1 within mitochondria upon OXPHOS perturbation. The ATP-dependent protease LONP-1 degrades the majority of ATFS-1 once the bZIP protein has been imported into the mitochondrial matrix¹⁹. LONP-1 is an ATP-dependent protease known to recognize and degrade mitochondrial proteins damaged by reactive oxygen species (ROS)²⁷. LONP-1 has also been shown to interact with mtDNA in diverse species^{28, 29}, and regulate mtDNA replication^{30, 31}.

To further examine the interaction between LONP-1 and mtDNA in *C. elegans*, we generated a strain in which the C-terminus of LONP-1 was tagged with the FLAG epitope via genome editing (Fig. 3a and Extended Data Fig. 3a). Introduction of the FLAG epitope did not impair worm development or cause UPR^{mt} activation, suggesting it did not adversely affect LONP-1 function (Extended Data Fig. 3b,c). As expected, LONP-1 interacted with mtDNA in *C. elegans* as determined by LONP-1^{FLAG} ChIP-mtDNA qPCR (Fig. 3b). We next examined where in mtDNA LONP-1^{FLAG} binds in wildtype homoplasmic worms. LONP-1^{FLAG} ChIP-seq indicated that the protease was enriched at several G-rich sites throughout mtDNA (Fig. 3c), but was especially enriched within the NCR (Fig. 3d). Interestingly, the strongest LONP-1^{FLAG} peak within the NCR overlapped with the ATFS-1 binding site (Fig. 3d and Extended Data Fig. 3d) suggesting a potential role in mediating the ATFS-1-mtDNA and POLG-mtDNA interactions.

We next examined the impact of *lonp-1*(RNAi) on mtDNA accumulation in homoplasmic wildtype worms. When raised on *lonp-1*(RNAi), the binding of ATFS-1 to mtDNA increased by ~5-fold (Fig. 3e) which correlated with an increase in mtDNA content (Fig. 3f). ATFS-1::GFP also accumulates within mitochondria raised on *lonp-1*(RNAi) (Fig. 3g,h). Importantly, exposure to *lonp-1*(RNAi) also increased the binding of POLG to mtDNA (Fig. 3i), consistent with increased POLG accumulation (Extended Data Fig. 3e). Moreover, LONP-1 inhibition increased mtDNA content in *atfs-1^{nuc}(-)* worms (Extended Data Fig. 3f), but not in *atfs-1(null)* worms (Fig. 3f).

To examine the role of mitochondrial-localized ATFS-1 in increasing mtDNA quantity, we sought to generate a strain lacking the MTS. Unfortunately, we were unable to establish a stable *atfs-1^{mts}(-)* line via genome editing. Thus, we generated *atfs-1^{mts}(-);nuc(-)* worms. Importantly, mtDNA copy number was not increased in *atfs-1^{mts}(-);nuc(-)* worms raised on *lonp-1*(RNAi) (Extended Data Fig. 3g) These findings support a role for mitochondrial-localized ATFS-1 in promoting mtDNA replication which is impaired by LONP-1-dependent degradation (Fig. 3j).

Nuclear ATFS-1 is not required to maintain heteroplasmy

We previously found that ATFS-1 is required to maintain mtDNAs^{9, 16} in a heteroplasmic worm strain using *atfs-1*(RNAi) and a hypomorphic *atfs-1* allele. Here, we crossed the *atfs-1(null)* allele into *uaDf5* heteroplasmic worms. Impressively, *atfs-1(null)* worms were unable to maintain any mtDNAs (Fig. 4a). The loss of mtDNAs in the absence of *atfs-1* may be due to increased mitophagy of mitochondria harboring mtDNAs^{16, 32},

decreased replication of mtDNAs, or a combination. To examine the role of mitophagy, we generated heteroplasmic strains lacking the mitophagy component Parkin (PDR-1 in worms) (Extended Data Fig. 4a). As expected, *pdr-1*-deficient worms had increased mtDNAs relative to wildtype worms consistent with mitophagy limiting the accumulation of mtDNAs^{9, 16}. *atfs-1(null);pdr-1(tm598)* worms also had significantly less mtDNAs than *pdr-1(tm598)* worms, indicating that ATFS-1 promotes heteroplasmy via a mechanism independent of mitophagy (Fig. 4a).

As OXPHOS perturbation increased mtDNA content in homoplasmic wildtype worms via ATFS-1, we hypothesized that OXPHOS dysfunction may contribute to the increased mtDNA content in heteroplasmic worms (Fig. 1d). We previously found that heteroplasmic worms consumed less oxygen than wildtype worms⁹. To further evaluate mitochondrial function, we examined mitochondrial membrane potential by staining with TMRE. As expected, TMRE staining was decreased in heteroplasmic worms relative to wildtype worms, but stronger than in *cco-1(RNAi)*- or *spg-7(RNAi)*-treated worms consistent with intermediate OXPHOS function (Fig. 2b, 4b and Extended Data Fig. 4b). Importantly, ATFS-1 also accumulated within the mitochondrial fraction of heteroplasmic worms, as in worms raised on *spg-7(RNAi)* or *cco-1(RNAi)* (Fig. 4c, also see Fig. 2a). Similar to homoplasmic worms raised on *cco-1(RNAi)*, ATFS-1::GFP accumulated within mitochondria with reduced TMRE staining in heteroplasmic worms. However, numerous mitochondria were TMRE positive, but the majority of those mitochondria lacked ATFS-1::GFP consistent with ATFS-1 being degraded in functional mitochondria (Fig. 4d). Combined, these results suggest that ATFS-1 accumulates within dysfunctional mitochondria caused by impairment of either a nuclear-encoded OXPHOS component, a nuclear-encoded mitochondrial protease, or in worms harboring mtDNAs.

We next examined if maintenance of mtDNAs required the nuclear activity of ATFS-1. Consistent with impaired nuclear activity, *hsp-6_{pr}::gfp* was not increased in heteroplasmic *atfs-1^{nuc(-)}* worms (Extended Data Fig. 4c,d). Impressively, unlike *atfs-1(null)* worms, *atfs-1^{nuc(-)}* worms were able to maintain mtDNAs although fewer mtDNAs than wildtype *atfs-1* worms (Extended Data Fig. 4e). To examine the role of mitochondrial-localized ATFS-1 during heteroplasmy, we crossed the *atfs-1^{mts(-);nuc(-)}* allele into heteroplasmic worms. *atfs-1^{mts(-);nuc(-)}* worms harbored fewer mtDNAs than *atfs-1^{nuc(-)}* worms emphasizing the requirement for mitochondrial localized ATFS-1 to maintain heteroplasmy (Extended Data Fig. 4f).

Consistent with the accumulation of ATFS-1 in dysfunctional mitochondria (Fig. 2a and 4b–d), ATFS-1 bound more total mtDNAs in heteroplasmic worms than in wildtype homoplasmic worms as determined by ChIP-mtDNA (Fig. 4e). Similarly, POLG also interacted with more total mtDNAs in heteroplasmic worms than in wildtype homoplasmic worms suggesting increased mtDNA replication (Extended Data Fig. 4g). Combined, these findings suggest a role for mitochondrial-localized ATFS-1 in maintaining deleterious mtDNA heteroplasmy.

ATFS-1 and POLG primarily bind mtDNAs

We next sought to determine if ATFS-1 differentially interacted with each genome. The interaction between ATFS-1 and wildtype mtDNAs or mutant mtDNAs was evaluated via qPCR or 3D digital PCR following ATFS-1 ChIP (Fig. 4f)⁹. As before, qPCR of mtDNA from heteroplasmic whole worm lysate indicated the strain harbored ~60% mutant mtDNAs and ~40% wildtype mtDNAs (Fig. 1b and Extended Data Fig. 5a). qPCR following ATFS-1 ChIP indicated that of the mtDNAs that interacted with ATFS-1, 90% were mutant mtDNAs and 10% were wildtype mtDNAs, indicating that ATFS-1 is significantly enriched on mutant mtDNAs (Fig. 4g and Extended Data Fig. 5b,c).

Previously, we found that inhibition of POLG caused depletion of mutant mtDNAs in heteroplasmic worms relative to wildtype mtDNAs⁹ similar to findings in a *Drosophila* heteroplasmy model⁸. Both findings suggest increased replication of mutant mtDNAs in heteroplasmic cells. To further explore the relationship between ATFS-1 and mtDNA replication, we performed ChIP-mtDNA using the POLG antibody. Interestingly, POLG ChIP indicated that the replicative polymerase also interacted with ~90% mutant mtDNAs and 10% wildtype mtDNAs (Fig. 4h and Extended Data Fig. 5d,e), similarly to ATFS-1 (Fig. 4g). As a control, we generated antibodies to the mtDNA packaging protein HMG-5 (TFAM in mammals) (Extended Data Fig. 5f,g), which interacts with mtDNAs independent of replication³³. In contrast to ATFS-1 and POLG, the percentage of mutant mtDNAs bound to HMG-5 reflected the percentage within the whole worm lysate (Fig. 4i). Combined, these data indicate that ATFS-1 and a component of the replisome are enriched on mutant mtDNAs in heteroplasmic worms, consistent with the mutant mtDNA having a replicative advantage.

The protease LONP-1 is required to maintain heteroplasmy

Because LONP-1 binds mtDNA and its proteolytic activity limits ATFS-1 accumulation in functional mitochondria¹⁹ (Fig. 3d,e), we examined the role of LONP-1 in heteroplasmy maintenance. We generated antibodies to *C. elegans* LONP-1 that recognized a ~130 KD band that was reduced when raised on *lonp-1*(RNAi) (Extended Data Fig. 6a). Via ChIP-qPCR, we found that LONP-1 binds ~60 fold more mutant mtDNAs than ATFS-1 in wildtype worms (Extended Data Fig. 6b). In heteroplasmic worms, LONP-1 bound similar percentages of wildtype and mutant mtDNAs suggesting that LONP-1 interacts with mtDNAs independent of mitochondrial dysfunction (Fig. 5a and Extended Data Fig. 6c). Combined, these data suggest that LONP-1 is constitutively bound to mtDNAs and heteroplasmy is not maintained by uneven mtDNA binding by the protease.

We next examined the effect of inhibiting LONP-1 on heteroplasmy. Interestingly, *lonp-1* inhibition via RNAi increased wildtype mtDNAs (Fig. 5b) and reduced mutant mtDNAs, which improved the heteroplasmy ratio from 59% mutant mtDNAs to 25% (Fig. 5c). Similar results were obtained in *atfs-1^{nuc(-)}* worms upon LONP-1 inhibition (Extended Data Fig. 6d). Importantly, *lonp-1*(RNAi) did not reduce the brood size of heteroplasmic worms (Extended Data Fig. 6e), suggesting that *lonp-1*(RNAi) did not select against embryos with dysfunctional mitochondria due to high levels of mutant mtDNAs.

We next examined the interaction between ATFS-1 and mtDNAs in heteroplasmic worms upon *lonp-1* inhibition. Interestingly, when raised on *lonp-1*(RNAi), the percentage of mtDNAs and wildtype mtDNAs bound to ATFS-1 nearly reflected the heteroplasmy percentage within the whole worm lysate (Fig. 5d). Consistent with the increased binding of ATFS-1 to wildtype mtDNAs, *lonp-1*(RNAi) increased ATFS-1::GFP accumulation within functional mitochondria (Fig. 5e,f). Thus, the mtDNA-bound protease is required to establish the enriched interaction between ATFS-1 and mtDNAs.

In addition to increasing the percentage of wildtype mtDNAs bound by ATFS-1, *lonp-1*(RNAi) also increased the percentage of POLG that interacted with wildtype mtDNAs (Fig. 5g, also see Fig. 4h). However, *lonp-1*(RNAi) did not alter the percentage of HMG-5/TFAM bound to mtDNAs, consistent with HMG-5 interacting with all mtDNAs independent of replication (Extended Data Fig. 6f). Consistent with ATFS-1-dependent mtDNA replication occurring in dysfunctional mitochondria, when heteroplasmic worms were raised on *cco-1*(RNAi) or crossed into the *clk-1* mutant strain, wildtype mtDNAs were also specifically increased (Extended Data Fig. 6g,h).

Combined, these findings suggest that LONP-1-mediated proteolysis antagonizes the ability of mitochondrial ATFS-1 and POLG to stimulate mtDNA replication. LONP-1 activity may be compromised within mitochondrial compartments harboring mtDNAs, leading to ATFS-1 and POLG accumulation and mtDNA replication. We propose that globally inhibiting LONP-1 promotes ATFS-1-mediated mtDNA replication throughout the cell, not just in compartments enriched in mtDNAs, consequently leading to a recovery of wildtype mtDNAs.

LONP1 inhibition improves heteroplasmy in cybrid cells

Lastly, we examined if the role of LONP1 in maintaining mtDNAs is conserved in mammals by examining two human heteroplasmic cybrid cell lines³⁴. While cybrid cells are often used as models of deleterious mtDNA heteroplasmy, it is important to note that cybrid cells are cancer cells in which patient-derived heteroplasmic mtDNAs were introduced by cell fusion³⁴. One cybrid line harbors a single nucleotide transition (COXI G6930A) that introduces a premature stop codon in the cytochrome c oxidase subunit I gene, which was isolated from a patient with a multisystem mitochondrial disorder (Fig. 6a)³⁵. We also examined a cybrid line harboring a 4977 base pair deletion known as the “common deletion” which removes multiple OXPHOS genes and is associated with Kearns-Sayre Syndrome (KSS), progressive external ophthalmoplegia, cancer and aging (Fig. 6a)^{36–39}. We first examined the impact of LONP1 siRNA on heteroplasmy in the KSS cybrid line. Similar to inhibition of *C. elegans* LONP-1, inhibition of human LONP1 by siRNA for 4 days (Fig. 6b), resulted in a 1.5-fold increase of wildtype mtDNAs (Fig. 6c) while KSS mtDNAs were decreased ~2 fold (Fig. 6d), resulting in a shift in the heteroplasmy ratio from 57.5% to 25.6% (Fig. 6d).

To further investigate the impact of LONP1 protease activity on heteroplasmy, we used the LONP1 inhibitor CDDO (2-cyano-3,12-dioxo-oleana-1,9(11)-dien-28-oic acid), also known as Bardoxolone (Fig. 6e)^{20,40}. As determined by deep sequencing, the CoxI G6930A cybrid line initially harbored ~90% G6930A mutant mtDNAs and ~10% wildtype mtDNAs (Fig.

6f). Interestingly, incubation with 0.1 μM or 0.25 μM CDDO for 3 weeks resulted in depletion of the CoxI G6930A mtDNA from 86% to 68% and 72%, respectively, with a concomitant increase in wildtype mtDNAs (Fig. 6f). Furthermore, continuous incubation with 0.1 μM or 0.25 μM CDDO for 18.5 weeks further decreased the heteroplasmic ratios from ~90% to ~47% and 62%, respectively (Fig. 6f and Extended Data Fig. 7a). Similar results were obtained when the KSS cybrid cells were incubated with CDDO. As determined by qPCR, KSS cells initially harbored ~50% mtDNAs. Incubation with 0.1 μM or 0.25 μM CDDO for 4 weeks depleted mtDNAs to 19.5% and 20.3% (Fig. 6g) and incubation for 13 weeks further depleted mtDNAs to 18.6% and 10.7%, respectively (Fig. 6g). Importantly, neither 0.1 μM nor 0.25 μM CDDO affected basal respiration in homoplasmic 143b cells (Extended Data Fig. 7b). Furthermore, neither used CDDO concentration impaired the viability of CoxI G6930A or KSS cells (Fig. 6h and Extended Data Fig. 7c) suggesting that the improved heteroplasmy ratio following CDDO exposure was not due to selection against cells with high levels of mutant mtDNAs. However, it remains possible that cell death may occur during longer exposures.

Last, we determined the impact of the CDDO-dependent shifts in heteroplasmy on OXPHOS. Impressively, incubation of KSS cells with 0.1 μM or 0.25 μM CDDO for 4 or 13 weeks resulted in significant increases in basal respiration suggesting improved OXPHOS (Extended Data Fig. 7d). The improved heteroplasmy caused by CDDO in CoxI G6930A cells (Fig. 7a) also resulted in increased basal respiration and maximal respiratory capacity (Fig. 7b–d). For example, 3 weeks exposure to 0.1 μM CDDO increased basal oxygen consumption ~2-fold, while exposure for 18.5 weeks improved basal oxygen consumption over 3-fold (Fig. 7b,c). Taken together, these findings suggest that inhibition of LONP1 improves deleterious heteroplasmy and recovers mitochondrial respiration. Notably, these phenotypes are independent of mtDNA length, as maintenance of mutant mtDNAs with either a large deletion or a single base pair substitution require LONP1 function.

Discussion

The underlying mechanisms that govern heteroplasmy dynamics are largely unknown, however it has been proposed that the mutant genomes have a selective advantage. Previously, we and others reported that heteroplasmy requires *atfs-1*^{9, 16}. In wildtype homoplasmic worms raised under normal conditions, ATFS-1 is imported into mitochondria and degraded by the protease LONP-1¹⁹. However, during mitochondrial dysfunction, a percentage of ATFS-1 accumulates within mitochondria and binds mtDNA¹⁷. Here, we report that mitochondrial-localized ATFS-1 promotes the accumulation of mtDNAs upon OXPHOS perturbation. Importantly, both ATFS-1 and POLG binding to mtDNA was increased upon OXPHOS perturbation. Consistent with this model, the nuclear activity of ATFS-1 is not required for the increased mtDNAs caused by OXPHOS perturbation in homoplasmic worms. Collectively, these results suggest that mitochondrial accumulation of ATFS-1 promotes recruitment of the mitochondrial replisome to mtDNA during OXPHOS dysfunction.

ATFS-1 is also required for the increased quantity of mtDNAs in heteroplasmic worms. The *uaDf5* strain harbors approximately 60% mtDNAs and 40% wildtype mtDNAs. However,

ATFS-1 and POLG interact with 9-fold more mtDNAs than wildtype mtDNAs suggesting the increase in total mtDNAs is due to increased mtDNA replication. As both mtDNAs harbor the ATFS-1 binding site, how is the specificity attained? We find that heteroplasmic worms harbor distinct populations of functional and dysfunctional mitochondria. And, ATFS-1 primarily accumulates within the dysfunctional population. Importantly, LONP-1 inhibition results in ATFS-1 accumulation in all mitochondria suggesting that the replicative advantage is due to LONP-1-dependent degradation of ATFS-1 in functional mitochondria, which likely harbor wildtype mtDNAs. Somatic cells in *C. elegans* harbor between one and three mtDNAs⁷. Thus, we speculate that the dysfunctional mitochondria in which ATFS-1 accumulates harbor all, or nearly all mtDNAs which impair OXPHOS and LONP-1, resulting in ATFS-1 accumulation.

Because LONP-1 is an ATP-dependent protease that degrades proteins damaged by ROS²⁷, mitochondrial dysfunction may impede degradation of ATFS-1 by LONP-1, resulting in recruitment of POLG to mtDNA. We propose that this mechanism evolved to coordinate mtDNA replication with expansion of the mitochondrial network during normal cell growth or recovery from mitochondrial dysfunction. However, if compartmental dysfunction is caused by an enrichment of mtDNAs, they are inadvertently, but preferentially, replicated. Our data suggests that inhibiting LONP1 throughout the mitochondrial network negates this preferential replication, leading to a reduction in the heteroplasmic ratio and recovery of mitochondrial function.

There are currently no FDA-approved treatments for diseases caused by mutant mtDNAs. However, the mTOR inhibitor rapamycin improves heteroplasmy in cybrid cells by increasing autophagy⁴¹. Of note, inhibition of several TORC1 components also inhibits *atfs-1*-dependent mitochondrial biogenesis in *C. elegans*¹⁸ suggesting TORC1 may function upstream of ATFS-1 in maintaining heteroplasmy. Here, we report that inhibition of LONP1 through siRNA-mediated knockdown or the small-molecule inhibitor CDDO reduces mtDNA abundance in cybrid cells harboring patient-derived mutant mtDNAs. Moreover, this decrease in mtDNAs was accompanied by improved mitochondrial respiration suggesting LONP1 inhibition may represent a therapeutic strategy for diseases caused by mutant mtDNAs.

Method

Materials and Methods

Worm strains—The reporter strain *hsp-6_{pr}::gfp* for visualizing UPR^{mt} activation was previously described²⁴. N2 (wildtype), and mtDNA (or *uaDf5*) strains were obtained from the *Caenorhabditis* Genetics Center (Minneapolis, Minnesota). The *atfs-1(et18)* strain was a gift from Mark Pilon. The *atfs-1(null)*, or *atfs-1(cmh15)*, strain was generated via CRISPR-Cas9 in wildtype worms as previously described²⁴. The crRNAs (Integrated DNA Technologies) were co-injected with purified Cas9 protein, tracrRNA (Integrated DNA Technologies), and the *dpy-10* co-injection marker as described⁴². *atfs-1^{mtuc(-)}* was introduced into both wildtype worms and the *hsp-6_{pr}::gfp* reporter strain via CRISPR-Cas9¹⁸ (crRNAs and replacement sequence listed in Supplementary Table 1). *lonp-1^{FLAG}* was introduced into both wildtype worms and the *hsp-6_{pr}::gfp* reporter strain via CRISPR-

Cas9. *atfs-1mts(-)* was introduced into to *atfs-1nuc(-)* worms to generate the *atfs-1mts(-);nuc(-)* strain. Each strain was outcrossed at least 5 times. Unless otherwise noted, all worms were harvested between the late L3 and early L4 stages. All strains were maintained at 20°C.

C. *elegans* mtDNA and human cybrid cell KSS mtDNA quantification—L4 wildtype or *uaDf5* worms were placed on agar plates seeded with control(RNAi) or RNAi specific to the described OXPHOS genes and the F1 generation was harvested at the L4 stage. Wildtype mtDNA or mtDNA quantification was performed using qPCR-based methods as described previously⁹. 40–60 worms were harvested in 35 µl of lysis buffer (50 mM KCl, 10 mM Tris-HCl (pH 8.3), 2.5 mM MgCl₂, 0.45% NP-40, 0.45% Tween 20, 0.01% gelatin, with freshly added 200 µg/ml proteinase K) and frozen at –80°C for 20 min prior to lysis at 65°C for 80 min. Relative quantification was used for determining the fold changes in mtDNA between samples. 1 µl of lysate was used in each triplicate qPCR reaction. qPCR was performed using the iQ™ SYBR® Green Supermix and the Biorad qPCR CFX96™ (Bio-Rad Laboratories). Primers that specifically amplify wildtype or mtDNA are listed in Supplementary Table 1, as are primers that amplify both wildtype and mtDNA (Total mtDNAs). Primers that amplify a non-coding region near the nuclear-encoded *ges-1* gene were used as an internal control for normalization (Supplementary Table 1).

For human patient fibroblast cell lines, wildtype and KSS primers were used to detect wildtype mtDNA or KSS mtDNA. Primers that amplify a sequence within the B2M (Human β2 myoglobin) gene were used as an internal control for normalization. Absolute quantification was also performed to determine the percentage or ratio of KSS mtDNA relative to total mtDNA (KSS mtDNA and wildtype mtDNA) as previously described⁹. Primers that specifically amplify wildtype or mtDNA are listed in Supplementary Table 1. Standard curves for each qPCR primer set were generated using purified plasmids individually containing approximately 1 kb of the mtDNA fragments specific for each primer set.

Chromatin immunoprecipitation (ChIP)—ChIP assays for ATFS-1 and LONP-1^{FLAG} were performed as previously described¹⁷. Synchronized worms were cultured in liquid and harvested at early L4 stage by sucrose flotation. The worms were lysed via Teflon homogenizer in cold PBS with protease inhibitors (Roche). Cross-linking of DNA and protein was performed by treating the worms with 1.85% formaldehyde with protease inhibitors for 15 min. Glycine was added to a final concentration of 125 mM and incubated for 5 min at room temperature to quench the formaldehyde. The pellets were resuspended twice in cold PBS with protease inhibitors. Samples were sonicated in a Bioruptor (Diagenode) for 15 min at 4°C on high intensity (30s on and 30s off). Samples were transferred to microfuge tubes and spun at 15,000*g for 15 min at 4°C. The supernatant was precleaned with pre-blocked ChIP-grade Pierce™ magnetic protein A/G beads (Thermo Scientific) and then incubated with Monoclonal ANTI-FLAG® M2 antibody (Sigma, F1804) or Mouse mAb IgG1 Isotype Control (Cell Signaling Technology, G3A1) rotating overnight at 4°C. The antibody-DNA complex was precipitated with protein A/G magnetic beads or protein A sepharose beads (Invitrogen). After washing, the crosslinks were reversed

by incubation at 65°C overnight. The samples were then treated with RNaseA at 37°C for 1.5 hour followed by proteinase K at 55°C for 2 hours. Lastly, the immunoprecipitated and input DNA were purified with ChIP DNA Clean & Concentrator (Zymo Research, D5205) and used as templates for qPCR or next generation sequencing.

mtDNA-immunoprecipitation (mtDNA-ChIP) and mtDNA quantification—

mtDNA-immunoprecipitation assays were performed similarly to the previously described ATFS-1 ChIP assay as described¹⁷. Synchronized worms were cultured in liquid and harvested at the L4 stage by sucrose flotation. The worms were lysed via Teflon homogenizer in cold PBS with protease inhibitors (Roche). Cross-linking of DNA and protein was performed by treating the worms with 1.85% formaldehyde along with protease inhibitors for 20 min at room temperature. Glycine was added to a final concentration of 125 mM and incubated for 5 min at room temperature to quench the formaldehyde. The pellets were washed twice in cold PBS with protease inhibitor. Samples were resuspended in 500 µl FA buffer + 0.1% sarkosyl* + protease/phosphatase inhibitors and transferred to new microfuge tubes and spun at 15,000*g for 15 min at 4°C. The lysates were not sonicated so that wildtype and mtDNA could be quantified by qPCR. The supernatant was precleaned with pre-blocked ChIP-grade PierceTM magnetic protein A/G beads (Thermo Scientific) and then incubated with the described antibodies rotating overnight at 4°C. The antibody-mtDNA complex was precipitated with protein A/G magnetic beads (Thermo Scientific) (LONP-1^{FLAG}) or protein A sepharose beads (Invitrogen) for ATFS-1, POLG, TFAM or LONP-1 antibodies. Sonicated salmon sperm DNA was used to block non-specific DNA binding on beads). Beads were collected and washed as previously described⁴³. After washing, the crosslinks were reversed by incubation at 250 mM NaCl 65°C overnight. The samples were then treated with RNaseA at 37°C for 1.5 hours and then proteinase K at 55°C for 2 hours. Lastly, the samples were purified with ChIP DNA Clean & Concentrator (Zymo Research, D5205) and used as templates for qPCR. The results were normalized by input and either non-specific rabbit IgG or mouse IgG1 was used as a negative control. Primers that amplify wildtype, mtDNA, or all mtDNAs (Total mtDNAs) are in Supplementary Table 1.

ChIP-seq analysis—The DNA fragments were sequenced using MiSeq at the University of Massachusetts Medical School Deep Sequencing Core. The quality of the raw sequencing data was first evaluated with fastqc (0.11.5). (<https://www.bioinformatics.babraham.ac.uk/projects/fastqc/>), and then mapped to the *C. elegans* genome (ce10 from UC Santa Cruz) by Burrows-Wheeler Aligner (BWA MEM, BWA version 0.7.15) algorithm with the standard default settings⁴⁴. Duplicate reads were removed using picard tools v1.96 (<https://broadinstitute.github.io/picard/>). Peaks were determined using MACS version 2.1⁴⁵ with the no-model parameter. Input was used as a control for peak-calling. Both narrow Peaks and broad Peaks were called, and the bigwig files were generated with the signal as fold enrichment by macs2 following the procedure at <https://github.com/taoliu/MACS/wiki/Build-Signal-Track>. The final set of peaks was determined if the difference in intensity values of control sample and input had a significance level of p-value < 0.01. IGV was used to view the peaks and signals. To identify candidate LONP-1 interacting motifs, the regions that were highly enriched were used as input for MEME (<http://meme.sdsc.edu>). MEME

was run using the parameters minw=8, maxw=25, in two modes (zoops & anr) and the significant motifs (E-value $\geq 1e-01$). A background model is used by MEME to calculate the log likelihood ratio and statistical significance of the motif.

Target site SNP frequency analysis in CoxI G6930A cells by deep sequencing

—Library construction for deep sequencing was modified from our previous report⁴⁶. Following CDDO treatment, cells were harvested at different time points and genomic DNA extracted. Briefly, regions flanking the CoxI G6930A site were PCR amplified using locus-specific primers bearing tails complementary to the Truseq adapters as described previously⁴⁷. 50–100 ng input genomic DNA (mtDNA included) was PCR amplified with Phusion High Fidelity DNA Polymerase (New England Biolabs): (98°C, 15 s; 67°C 25 s; 72°C 18 s) \times 30 cycles. 1 μ l of each PCR reaction was amplified with barcoded primers to reconstitute the TruSeq adapters using the Phusion High Fidelity DNA Polymerase (New England Biolabs): (98°C, 15 s; 61°C, 25 s; 72°C, 18 s) \times 9 cycles. Equal amounts of the products were pooled and gel purified. The purified library was deep sequenced using a paired-end 150 bp Illumina MiSeq run.

MiSeq data analysis for editing at target sites or off-target sites was performed using a suite of Unix-based-software tools. First, the quality of the paired-end sequencing reads (R1 and R2 fastq files) was assessed using FastQC (<http://www.bioinformatics.babraham.ac.uk/projects/fastqc/>). Raw paired-end reads were combined using paired end read merger (PEAR)⁴⁸ to generate single merged high-quality full-length reads. Reads were then filtered by quality (using Filter FASTQC⁴⁷) to remove those with a mean PHRED quality score under 30 and a minimum per base score under 24. Each group of reads was then aligned to a corresponding reference sequence using BWA (version 0.7.5) and SAMtools (version 0.1.19). To determine background SNP or sequencing errors, all reads from each negative control replicate were combined and aligned, as described above. Background SNP types and frequencies were then cataloged in a text output format at each base using bam-readcount (<https://github.com/genome/bam-readcount>). For each drug treatment group, the average background SNP frequencies (based on SNP type, position and frequency) of the triplicate negative control group were subtracted to obtain the accurate SNP frequencies.

QuantStudio 3D Digital PCR—The detailed method was described previously⁴⁹. All primers and probes were ordered from IDT (Coralville, Iowa). The 3D digital PCR was used according to the manufacturer's protocol. QuantStudio™ 3D Digital PCR Master Mix v2 and individual QuantStudio 3D digital PCR 20K Chip kit v2 were purchased from Thermo scientific (Applied Biosystems, Waltham, MA). Prepared sample mix was loaded into CHIP using QuantStudio 3D Digital PCR Chip Loader (Thermo scientific). Chip PCR amplification was performed in a ProFlex PCR System (96 °C for 10 min; 39 cycles of 60 °C for 2 min and 98 °C for 30 sec; and 60 °C for 2 min). After amplification, each chip was loaded into the QuantStudio 3D Digital reader. Data were analyzed using QuantStudio 3D Analysis Suite (Thermo scientific). All biological repeats were performed in at least triplicate.

mtDNA primers F: TTGCTTTTTCTTTATATGTTTTG; R: TTTATTTAATTTGGTTAAACAAGAGGT. mtDNA probes 5' 6-FAM/ZEN/3' IBFQ: /56-FAM/AGGATCGTA/ZEN/ACATTTTATTTTTTGCTTTA/3IABkFQ/.
 Wildtype primers F: GCTTTTTCTTTATATGTTTTGTG.
 R: TCACCTTCAGAAAAATCAAATGG wildtype mtDNA probes 5' HEX/ZEN/3' IBFQ: /5HEX/AATTATAGT/ZEN/AATTGCTGAACCTAACCGGGC/3IABkFQ/

RNA isolation and qRT-PCR—Total RNA was isolated from worm pellets using the TRIzol™ Reagent (Invitrogen). cDNA was then synthesized from total RNA using the iScript cDNA Synthesis Kit (Bio-Rad). qPCR was performed to determine the expression levels of the indicated genes using iQ™ SYBR GREEN supermix (Bio-Rad). Primer sequences are listed in Supplementary Table 1. Relative expression of target genes was normalized to the control. Fold changes in gene expression were calculated using the comparative Ct - Ct method as previously described¹⁷.

Chemicals and Antibodies—CDDO (Cayman Chemicals Cat No 81035). ATFS-1 polyclonal antibodies were generated and validated previously¹⁹. Polyclonal antibodies were generated to amino acid amino acids 1054–1072 of *C. elegans* POLG and subsequently affinity purified by Thermo Fisher Scientific Inc. Polyclonal antibodies were generated to amino acid amino acids 191–204 of *C. elegans* HMG-5 (TFAM) and subsequently affinity purified by Thermo Fisher Scientific Inc. Polyclonal antibodies were generated to amino acid amino acids 953–971 of *C. elegans* LONP-1 and subsequently affinity purified by Thermo Fisher Scientific Inc. Monoclonal anti-FLAG® M2 antibody (Sigma, Cat # F1804), α -tubulin (Sigma), NDUFS3 (NUO-2 in *C. elegans*, complex I, Abcam). Supplementary Table 2.

Cell Culture—The KSS cell line was a gift from Carlos Moraes^{36, 37}. The CoxI C6930A cell line was a gift from Giovanni Manfredi³⁵. Cells were cultured in DMEM (4mM L-glutamine, 4.5 g/L glucose; Gibco, Thermo Fisher Scientific) plus 10% FBS with 1% pen-strep. Total cellular mtDNA was prepared as described⁵⁰. Cells were incubated continuously in the described concentration of CDDO for the indicated number of days. The cells were sub-cultured prior to confluence every 48 hours.

Cell Viability—At the indicated time points, cells were stained with trypan blue⁵¹ and quantified with an automated cell counter TC-20™ (Bio-Rad). The results are an average of three independent assays.

siRNA—Cells were grown in 6-well plates and siRNAs were transfected with Lipofectamine RNAiMAX (Thermo Fisher Scientific Cat No 13778150) following the manufacturer's instructions. Human LONP1 siRNA was purchased from Dharmacon (L-003979-00-0005).

Respiration Assays—For mitochondrial respiration assays, oxygen consumption rate (OCR) was measured using a Seahorse Extracellular Flux Analyzer XFe96 (Seahorse Biosciences) as described⁵⁰. 14,000 CoxI G6930A cells were seeded per well with

fresh medium. OCR was measured using the Cell MitoStress Kit (as described by the manufacture). 180 μ l of XF-Media was added to each well and then the plates were subjected to analysis following sequential introduction of 1.5 μ M oligomycin, 1.0 μ M FCCP and 0.5 μ M rotenone/antimycin as indicated. Data is normalized to total protein as determined by the BCA protein assay.

Western Blots and Mitochondrial Fractionation—Mitochondrial fractionation and western blots were performed as described previously¹⁷. Synchronized L4 worms were harvested from liquid culture by sucrose flotation. The worm pellets were approximately 150 μ l. The worms were washed two times in mitochondria buffer (70 mM sucrose, 1 mM EGTA, 210 mM sorbitol, 10 mM MOPS [pH 7.4])⁵² and resuspended in 300 μ l of mitochondria buffer. The worms were then homogenized with a dounce homogenizer at 4°C. 600 μ l of mitochondria buffer was added and the samples were centrifuged at 450 \times g for 10min at 4°C to pellet debris. The supernatant was collected and centrifuged at 550 \times g for 10min at 4°C to pellet the remaining debris. The supernatant was collected and 100 μ l was saved as the Total fraction. The rest of the supernatant was centrifuged at 9500 \times g for 10min at 4°C to pellet the mitochondria. The supernatant was saved as the Cytosolic fraction. The mitochondrial pellet was washed once in mitochondria buffer, resuspended in 1.5 ml mitochondria buffer and incubated on ice for 15 min. The sample was centrifuged at 500 \times g for 10min at 4°C. The supernatant was collected and again centrifuged at 9500 \times g for 10min at 4°C. The pellet was collected and resuspended in 100 μ l mitochondria buffer and saved as the Mitochondrial fraction.

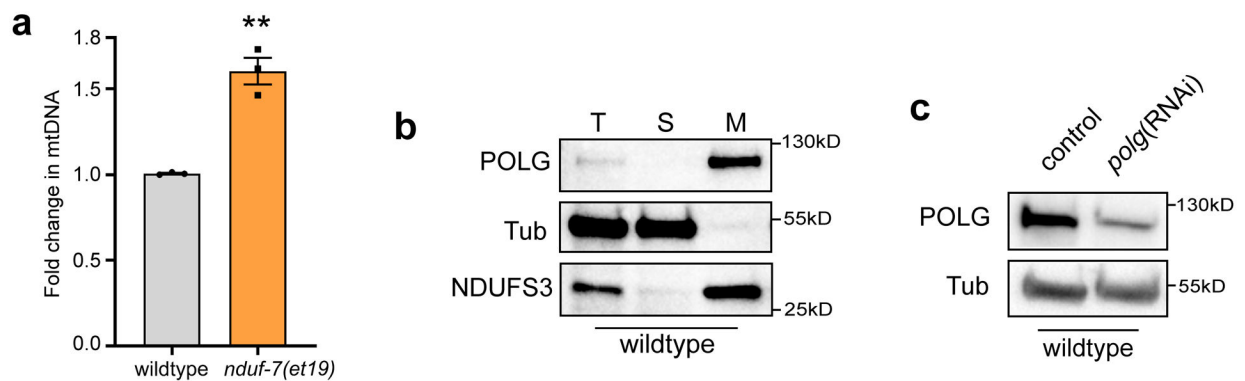
Imaging and Fluorescence Quantification—Whole worm images were obtained using either a Zeiss AxioCam MRm camera mounted on a Zeiss Imager Z2 microscope or a Zeiss M2BIO dissecting scope as described²⁴. TMRE staining was performed by synchronizing and raising worms on plates previously soaked with S-Basal buffer containing DMSO, or final concentration 100 μ M TMRE (Sigma, Cat No 87917). Prior to imaging, the TMRE-stained worms were transferred to plates seeded with control(RNAi) bacteria for 3 h to remove TMRE-containing bacteria from the digestive tract. Images were acquired using identical exposure times with a ZEISS LSM800 microscope with Airyscan. TMRE staining analysis was performed as described^{53, 54}. In short, the average pixel intensity values were calculated by sampling images of different worms. The average pixel intensity for each animal was calculated using ImageJ (<http://rsb.info.nih.gov/ij/>). The fluorescence pixel intensity was quantified by using the threshold-adjusted images from worms at each condition in biological triplicates. Mean values were compared using Student's t test or one-way (ANOVA) variance analysis followed by the post-hoc Tukey's test where appropriate.

ATFS-1::GFP transgenic worms were stained with TMRE as described above. Co-localization of TMRE stain and ATFS-1::GFP was determined by object-based colocalization analysis as described⁵⁵. The amount of co-localization was calculated for each sample. Statistical analysis was performed using the Prism software package (GraphPad Software).

Statistics and reproducibility—All data are reported as mean \pm SEM. Significance was accepted at $P < 0.05$. Asterisks denote corresponding statistical significance * $P <$

0.05; ** $P < 0.01$; *** $P < 0.001$ and **** $P < 0.0001$. No statistical method was used to predetermine the sample size. Results were analyzed using Student's t test with a two-tailed distribution or one-way ANOVA (for multiple comparison) where appropriate, using GraphPad Prism software with corrected P values < 0.05 considered significant. For multiple comparisons, P values were adjusted using the Tukey's post hoc. The statistical analyses for oxygen consumption rate (OCR) and ChIP-mtDNA assays were all performed using two-sided Student's t-tests; no adjustments were applied. The statistical tests performed and definition of " n " numbers in this study are indicated in the figure legends. For Figs. 1d,1g–1h, 2c,2e–2i, 3b, 3e–3f, 3h–3i, 4a,4e, 4g–4i, 5a–5d, 5f–5g, 6c,6d, 6g–6h, 7a–7d, and Extended Data Figs. 1a, 2c, 2f–h, 3f–g, 4e–g, 5c, 5e, 6b–h, 7b–d, " n " means biologically independent samples. For *C. elegans* western blotting and gene expression, each sample within each biological replicate corresponds to a sample pooled from 3000–5000 animals. For the immunoblotting data, each blot (Figs. 2a,2d,3a,4c,6b and Extended Data Figs. 1b–c,2i–j, 3e,5g) was repeated at least three times and each blot (Extended Data Fig. 5f) was repeated twice with similar results. In Figs. 1c,1e,1f,2b,3g,4b,4d; 5e, and Extended Data Figs. 2d,3b,3c,4c, these experiments were independently repeated at least three times. For cell culture western blotting, each sample within each biological replicate corresponds to one well from a tissue culture plate. For Figs. 7b–d and Extended Data Figs. 7d, " n " means biological replicates and each sample within each biological replicate corresponds to a sample pooled from 14000 cells in Fig. 7b–d, 18000 cells in Extended Data Fig. 7d (4 weeks) and 10000 cells (13 weeks). The deep sequencing to quantify heteroplasmy of the CoxI G6930A mtDNA following exposure to CDDO was double-blinded. The researchers involved in the experiments were not completely blinded during sample obtainment or data analysis.

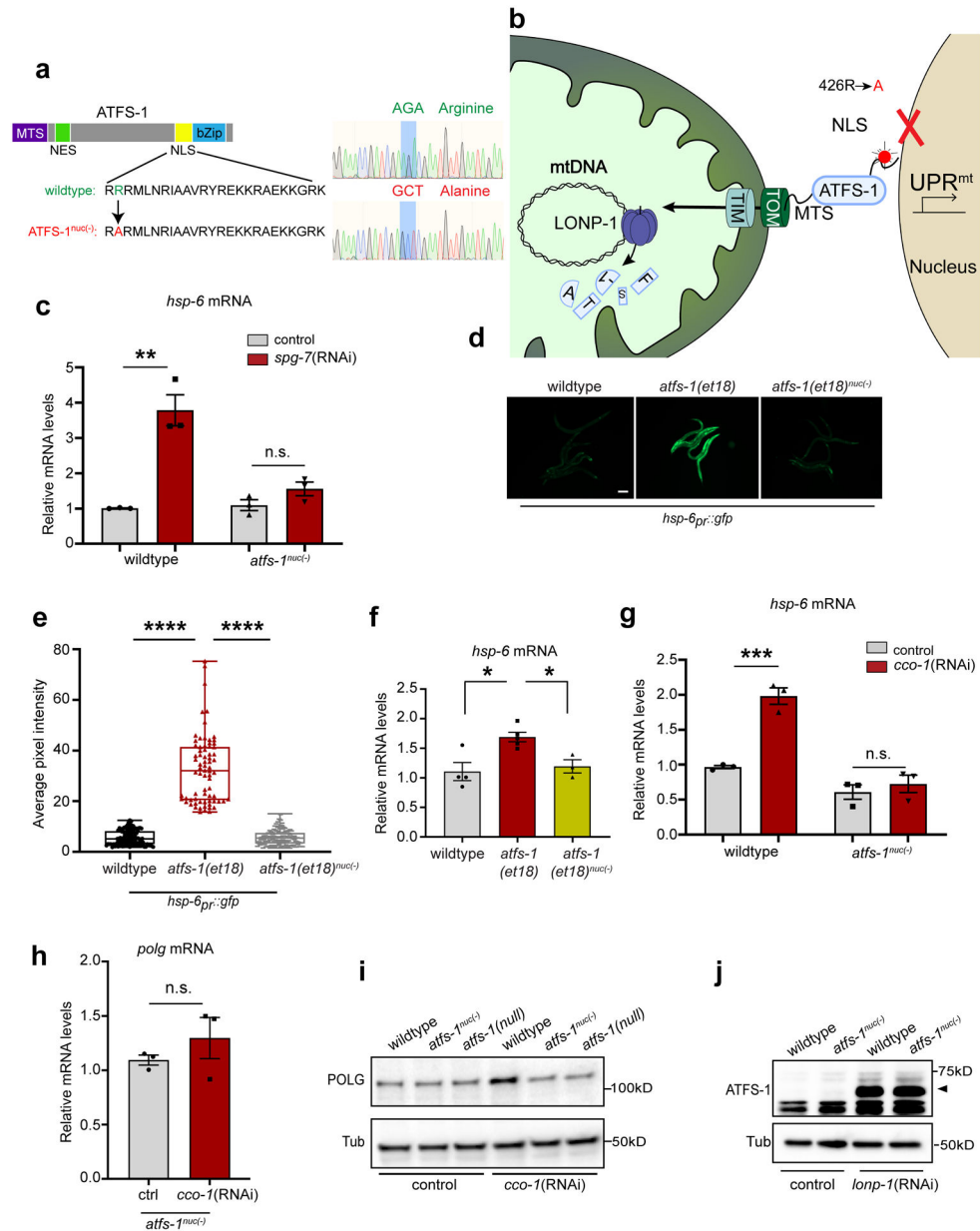
Extended Data



Extended Data Fig. 1. OXPPOS dysfunction increases mtDNAs

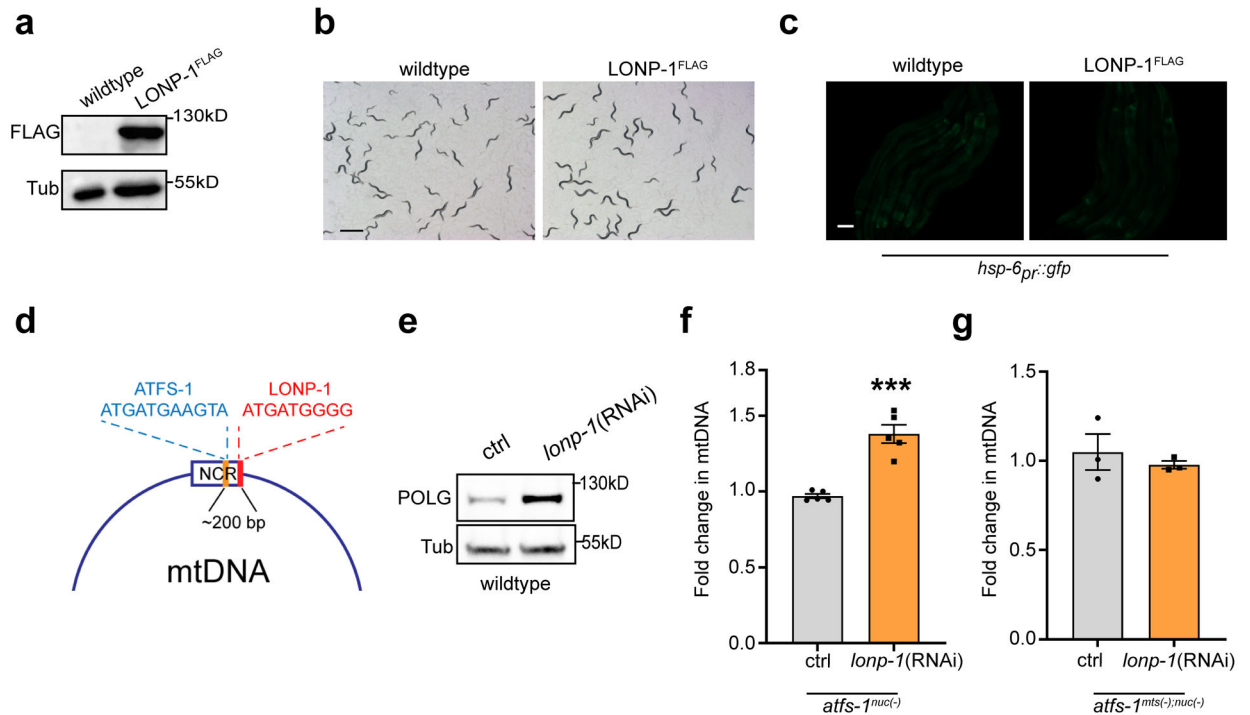
a, Quantification of total mtDNA in wildtype and *nduf-7(et19)* worms. $n = 3$, biologically independent samples (Each sample contains 40–60 animals; every dot stands for averaged value from 3 technical replicates; data shown represent mean \pm S.E.M.). ** $P = 0.0015$, Two-tailed Student's t test. **b**, POLG immunoblot of wildtype worms following fractionation into total lysate (T), post-mitochondrial supernatant (S), and mitochondrial pellet (M). Tubulin (Tub) and the OXPPOS protein (NDUFS3) serve as loading controls. Representative immunoblots from four biological repeats. **c**, POLG immunoblot of lysates from wildtype

worms raised on control(RNAi) or *polg*(RNAi). Tubulin (Tub) serves as a loading control. Representative immunoblots from seven biological repeats.



Extended Data Fig. 2. *atfs-1*-dependent transcription is impaired in *atfs-1^{nuc(-)}* worms.
a. Schematic highlighting the R (Arginine) to A (Alanine) substitution to impair the nuclear localization sequence (NLS) within ATFS-1 yielding ATFS-1^{nuc(-)} confirmed by Sanger sequencing. **b.** UPR^{mt} signaling schematic highlighting the ATFS-1^{nuc(-)} with an impaired NLS. **c.** Expression level of *hsp-6* mRNA in wildtype and *atfs-1^{nuc(-)}* worms raised on control(RNAi) or *spg-7*(RNAi) examined by qRT-PCR. *n* = 3, biologically independent samples. ***P* = 0.0028, One-way ANOVA. **d-e.** Photomicrographs of wildtype, *atfs-1(et18)* and *atfs-1(et18)^{nuc(-)}*; *hsp-6_{pr}::gfp* worms (Scale bar 0.1 mm) (**d**); Quantification

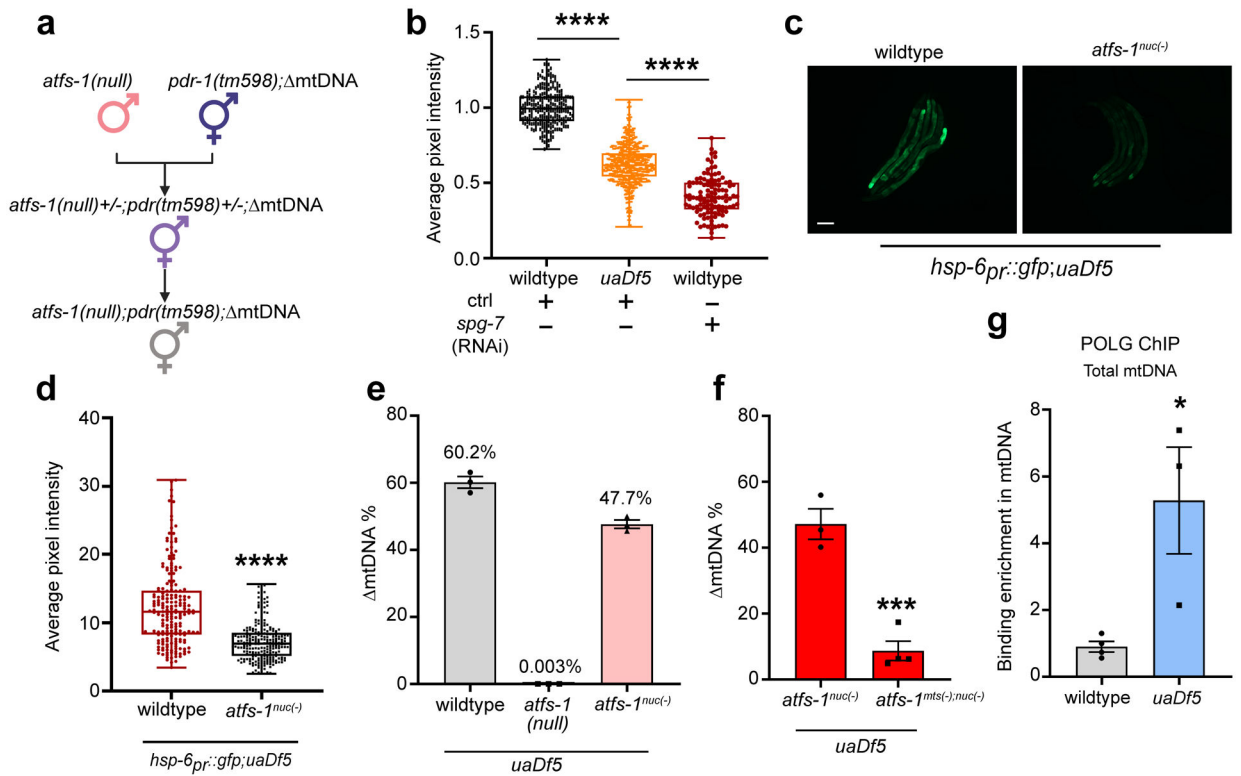
of fluorescence pixel intensity in wildtype ($n = 117$; Max: 12.51; Min: 1.87; Median: 5.12), *atfs-1(et18)* ($n = 74$; Max: 75.251; Min: 15.790; Median: 32.021) and *atfs-1(et18)^{nuc(-)}* strains ($n = 121$; Max: 15.100; Min: 1.55; Median: 5.43). Box & whiskers plots Min to Max. **** $P < 0.0001$, One-way ANOVA. n means the number of sampling areas. Average pixel intensity signals were calculated from sampling areas at each condition in biological triplicates (e). f, *hsp-6* mRNA expression in wildtype, *atfs-1(et18)* or *atfs-1(et18)^{nuc(-)}* worms examined by qRT-PCR. $n = 4$ (wildtype), $n = 5$ (*atfs-1(et18)*), $n = 3$ (*atfs-1(et18)^{nuc(-)}*), biologically independent samples. * $P = 0.0114$ (wildtype vs. *atfs-1(et18)*), * $P = 0.0407$ (*atfs-1(et18)* vs. *atfs-1(et18)^{nuc(-)}*), one-way ANOVA. g, *hsp-6* mRNA expression in wildtype and *atfs-1^{nuc(-)}* worms raised on control(RNAi) or *cco-1*(RNAi) examined by qRT-PCR. $n = 3$, biologically independent samples. *** $P = 0.0004$, one-way ANOVA. h, *polg* mRNA expression in *atfs-1^{nuc(-)}* worms raised on control(RNAi) or *cco-1*(RNAi) examined by qRT-PCR. $n = 3$, biologically independent samples. Two-tailed Student's t test. i, POLG immunoblots of lysates from wildtype, *atfs-1^{nuc(-)}* and *atfs-1(null)* worms raised on control or *cco-1*(RNAi). Representative immunoblots from four biological repeats. j, Immunoblots of lysates from wildtype and *atfs-1^{nuc(-)}* worms raised on control or *lonp-1*(RNAi). ATFS-1 or ATFS-1^{nuc(-)} are indicated with an arrowhead. Representative immunoblots from four biological repeats. In c, f-h, each dot represents the average from 3 technical replicates; data shown represent mean \pm S.E.M.



Extended Data Fig. 3. LONP-1 inhibition promotes mtDNA content via ATFS-1

a, FLAG immunoblots of lysates from wildtype and LONP-1^{FLAG} wildtype worms. Tubulin (Tub) serves as a loading control. Representative immunoblots from four biological repeats. **b**, Images of wildtype or LONP-1^{FLAG} worms 48 hours after synchronization indicating worms expressing LONP-1^{FLAG} at the endogenous locus develop normally (Scale bar 1

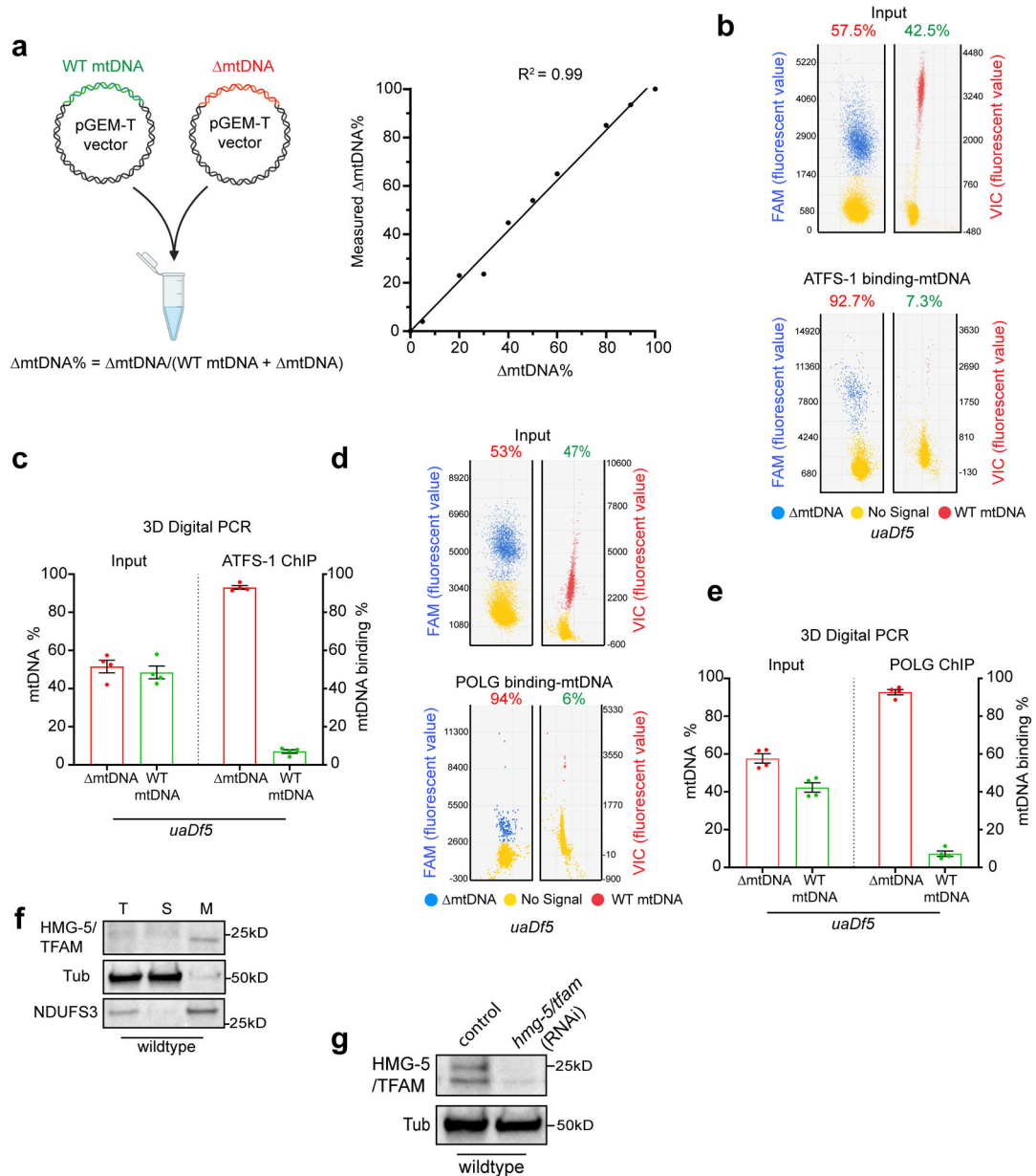
mm). Representative images from four biological repeats. **c**, Fluorescent photomicrographs of wildtype *hsp-6_{pr}::gfp* or *lonp-1^{FLAG};hsp-6_{pr}::gfp* worms 48 hours after synchronization indicating worms expressing LONP-1^{FLAG} do not cause UPR^{mt} activation (Scale bar 0.05 mm). Representative images from four biological repeats. **d**, Schematic of the putative ATFS-1 and LONP-1 binding sites within the mtDNA non-coding region (NCR) highlighting the proximity of both sites (~200 base pairs). **e**, POLG Immunoblots of lysates from wildtype worms raised on control or *lonp-1*(RNAi). Representative images from four biological repeats. **f**, Total mtDNA quantification in wildtype homoplasmic *atfs-1^{nuc(-)}* worms raised on control(RNAi) or *lonp-1*(RNAi). *n* = 5, biologically independent samples. ****P* = 0.0004, Two-tailed Student's t test). **g**, Total mtDNA quantification in wildtype homoplasmic *atfs-1^{mts(-);nuc(-)}* worms raised on control(RNAi) or *lonp-1*(RNAi). *n* = 3, biologically independent samples. Two-tailed Student's t test. In **f** and **g**, each biologically independent sample contained 40–60 animals; every dot stands for averaged value from 3 technical replicates; data shown represent mean ± S.E.M. **p*<0.05, ***p*<0.01, ****p*<0.0001.



Extended Data Fig. 4. Mitochondrial ATFS-1 is required to maintain mtDNA in heteroplasmic worms.

a, Crossing strategy of *atfs-1*(null);*pdr-1*(*tm598*);*uaDf5* strain. **b**, TMRE quantification of heteroplasmic (ΔmtDNA) worms raised on control(RNAi) (*n* = 475; Max: 1.052; Min: 0.21; Median: 0.618), or wildtype worms raised on control (*n* = 232; Max: 1.318; Min: 0.725; Median: 0.995) or *spg-7*(RNAi) (*n* = 114; Max: 0.798; Min: 0.134; Median: 0.402). Box & whiskers plots Min to Max. *n* means the number of sampling areas. Average pixel intensity signals were calculated from sampling areas at each condition in biological triplicates.

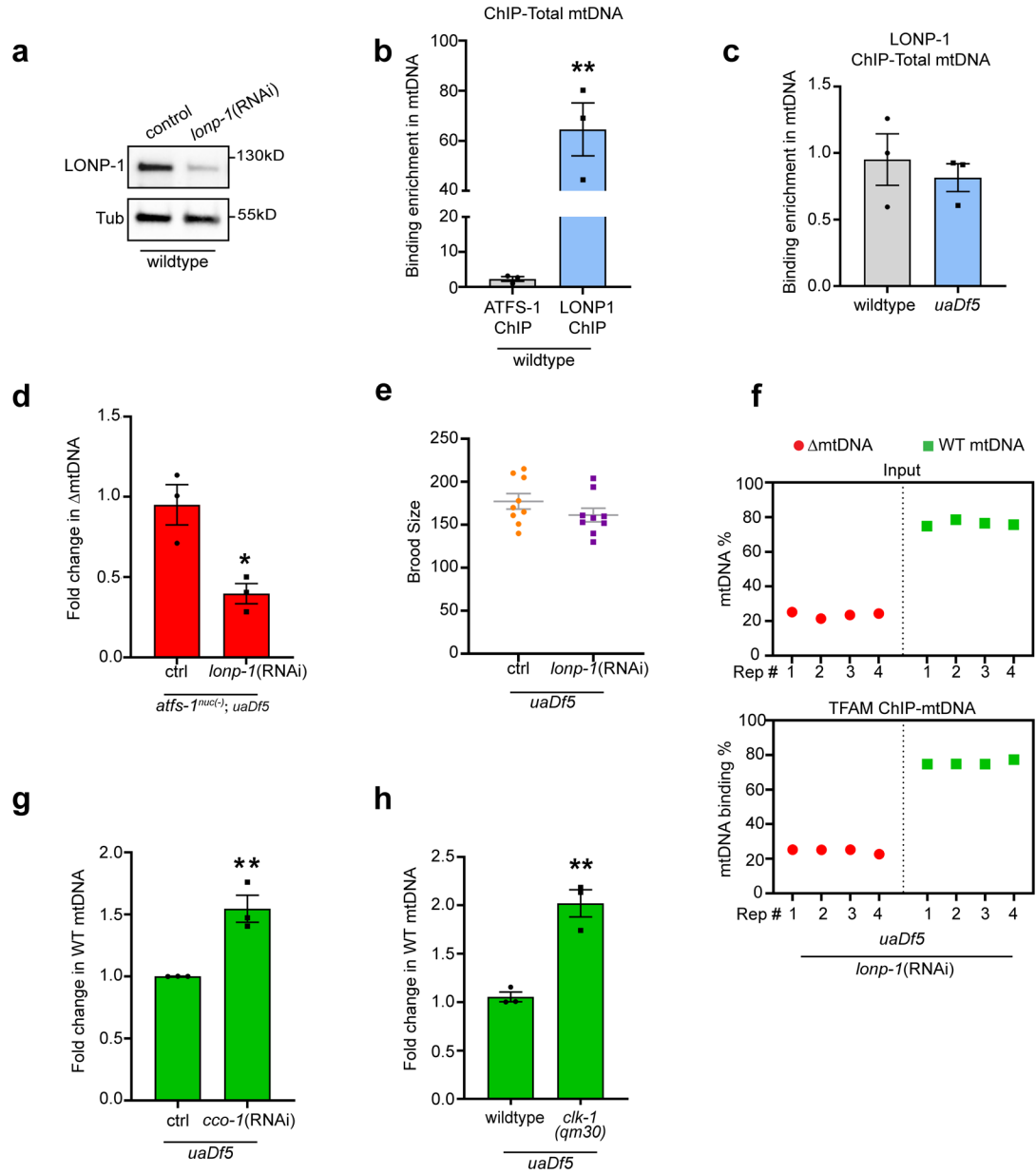
c,d, Photomicrographs of *uaDf5* and *atfs-1^{nuc(-)};uaDf5;hsp-6_{pr}::gfp* worms (Scale bar 0.1 mm) (**c**); Quantification of fluorescence pixel intensity in *uaDf5* ($n = 199$; Max: 30.89; Min: 3.430; Median: 11.590) and *atfs-1^{nuc(-)};uaDf5;hsp-6_{pr}::gfp* ($n = 234$; Max: 15.640; Min: 2.540; Median: 6.915). Box & whiskers plots Min to Max. n means the number of sampling areas. Average pixel intensity signals were calculated from sampling areas at each condition in biological triplicates (**d**). **e**, mtDNA quantification as determined by qPCR in heteroplasmic *uaDf5* worms, *atfs-1(null);uaDf5* worms and *atfs-1^{nuc(-)};uaDf5* worms. $n = 3$, biologically independent samples. **f**, mtDNA quantification as determined by qPCR in heteroplasmic *atfs-1^{nuc(-)};uaDf5* worms and *atfs-1^{mts(-);nuc(-)};uaDf5*. $n = 3$ (*atfs-1^{nuc(-)};uaDf5*) and $n = 4$ (*atfs-1^{mts(-);nuc(-)};uaDf5*), biologically independent samples. *** $P = 0.0007$. **g**, Quantification of total mtDNA following POLG ChIP-mtDNA in homoplasmic wildtype or *uaDf5* worms. $n = 4$ (wildtype) and $n = 3$ (*uaDf5*), biologically independent samples. * $P = 0.0229$. In **e** and **f**, each biologically independent sample contained 40–60 animals; in **g**, each biologically independent sample contained about 150,000 animals; each dot stands for averaged value from 3 technical replicates in **f,g**; Two-tailed Student's t test was used in **d, f** and **g**, One-way ANOVA was used in **b**; data shown represent mean \pm S.E.M. * $p < 0.05$, ** $p < 0.01$, **** $p < 0.0001$.



Extended Data Fig. 5. ATFS-1 and POLG primarily interact with mtDNAs in heteroplasmic worms.

a, Overview of the qPCR strategy to quantify the Δ mtDNA percentage in heteroplasmic worms or heteroplasmic cells. Plasmids containing a sequence specific to the Δ mtDNA or wildtype mtDNA were created²⁰. Standard curves were generated using the indicated concentration of each plasmid harboring sequences specific to either wildtype or Δ mtDNAs. Both PCR reactions were carried out simultaneously in the same qPCR machine. **b**, Scatter plots (**b**) and results (**c**) of 3D digital PCR quantification of wildtype mtDNA and Δ mtDNA following ATFS-1 ChIP-mtDNA in heteroplasmic *uaDf5* worms. $n = 4$, biologically independent samples. **d-e**, Scatter plots (**d**) and results (**e**) of 3D digital PCR quantification of wildtype mtDNA and Δ mtDNA following POLG ChIP-mtDNA in heteroplasmic *uaDf5* worms. $n = 4$, biologically independent samples. **f**, HMG-5/TFAM immunoblot of wildtype

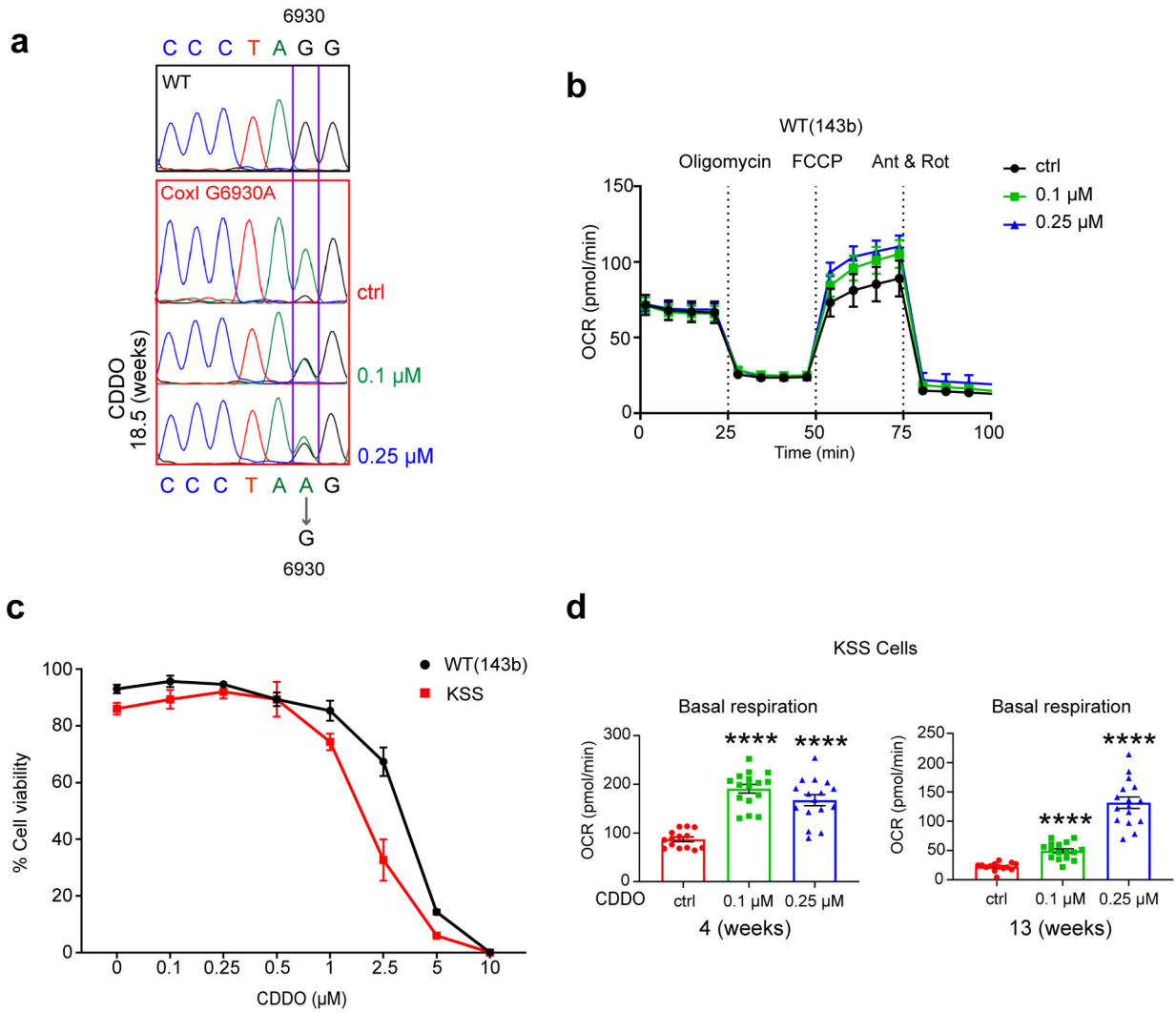
worms following fractionation into total lysate (T), post-mitochondrial supernatant (S), and mitochondrial pellet (M). Tubulin (Tub) and the OXPHOS component (NDUFS3) serve as loading controls. Representative immunoblots from two biological repeats. **g**, HMG-5/TFAM immunoblots of lysates from wildtype worms raised on control or *hmg-5/ tfam*(RNAi). Tubulin (Tub) serves as a loading control. Representative immunoblots from three biological repeats. Each biologically independent sample contained 150,000 animals in **c,e**; data shown represent mean \pm S.E.M.



Extended Data Fig. 6. Inhibition of LONP-1 improves the deleterious heteroplasmy ratio

a, LONP-1 immunoblots of lysates from wildtype worms raised on control(RNAi) or *lonp-1*(RNAi). Tubulin (Tub) serves as a loading control. Representative immunoblots from

four biological repeats. **b**, ChIP-mtDNA using ATFS-1 or LONP-1 antibodies in wildtype worms followed by quantification of total mtDNA. $n = 3$, biologically independent samples. $**P = 0.0042$. **c**, ChIP-mtDNA using LONP-1 antibodies in wildtype or heteroplasmic worms followed by quantification of total mtDNA (both wildtype and mtDNA). $n = 3$, biologically independent samples. **d**, mtDNA quantification in *atfs-1^{nuc(-)};uaDf5* worms raised on control(RNAi) or *lonp-1*(RNAi). $n = 3$, biologically independent samples. $*P = 0.0168$. **e**, The brood size of heteroplasmic worms raised on control or *lonp-1*(RNAi). $n = 9$ worms. **f**, mtDNA and wildtype mtDNA quantification following HMG-5/TFAM ChIP-mtDNA in *uaDf5* heteroplasmic worms raised on *lonp-1*(RNAi) indicating that the binding of HMG-5/TFAM to wildtype mtDNAs or mtDNAs is similar the input ratio. $n = 4$, biologically independent samples. **g**, wildtype mtDNA quantification in *uaDf5* heteroplasmic worms raised on control(RNAi) or *cco-1*(RNAi). $n = 3$, biologically independent samples. $**P = 0.0075$. **h**, wildtype mtDNA quantification in *uaDf5* or *clk-1(qm30);uaDf5* heteroplasmic worms. $n = 3$, biologically independent samples. $**P = 0.0029$. In **b,c** and **f**, Each biologically independent sample contained 150,000 animals; in **d,g,h** each biologically independent sample contained 40–60 animals; every dot stands for averaged value from 3 technical replicates in **b-d** and **f-h**; Two-tailed Student's t test was used; data shown represent mean \pm S.E.M.



Extended Data Fig. 7. Pharmacological inhibition of LONP1 improves heteroplasmy and OXPHOS function in heteroplasmic cybrid cells

a. Mutant (G6930A) mtDNA ratio confirmation by sanger sequencing in CoxI G6930A cells treated by CDDDO. **b.** Oxygen consumption rates (OCR) of 143B (wildtype) cells treated with DMSO (ctrl), 0.1 μM or 0.25 μM CDDDO for 3 days. *n* = 22 (ctrl) and *n* = 24 (0.1 μM and 0.25 μM CDDDO), biologically independent samples. **c.** Cell viability of 143b (WT) and KSS mtDNA cells exposed to various concentrations of CDDDO for 72 hours. *n* = 3, biologically independent samples. **d.** Basal respiration of KSS heteroplasmic cells treated with DMSO (ctrl), 0.1 μM or 0.25 μM CDDDO for 4 or 13 weeks. *n* = 14 (ctrl) and *n* = 16 (0.1 μM and 0.25 μM CDDDO), biologically independent samples. *****P* < 0.0001, Two-tailed Student's *t* test. Data shown represent mean ± S.E.M.

Supplementary Material

Refer to Web version on PubMed Central for supplementary material.

ACKNOWLEDGMENTS

We thank the Caenorhabditis Genetics Center for providing *C. elegans* strains (funded by NIH Office of Research 362 Infrastructure Programs (P40 OD010440). We thank Carlos Moraes for the KSS and Giovanni Manfredi for the CoxI G6930A cybrid cell lines.

Funding:

This work was supported by HHMI, the Mallinckrodt Foundation and National Institutes of Health grants (R01AG040061 and R01AG047182) to C.M.H., (R01GM115911 and R01AI117839) to S.A.W., (R01GM111706 and R35GM130320) to P.C. and (F31HL147482) to K.L.

Data availability

The ChIP-sequencing data have been deposited to the Gene Expression Omnibus database under the BioProject accession code PRJNA590136. The next-generation sequencing data at mtDNA have been deposited in the NCBI Sequence Read Archive database under the BioProject accession code PRJNA780293. Source data are provided with this study. All other data supporting the findings of this study are available from the corresponding author on reasonable request.

REFERENCES

1. Baker BM & Haynes CM Mitochondrial protein quality control during biogenesis and aging. *Trends in biochemical sciences* 36, 254–261 (2011). [PubMed: 21353780]
2. Wai T, Teoli D & Shoubridge EA The mitochondrial DNA genetic bottleneck results from replication of a subpopulation of genomes. *Nature genetics* 40, 1484–1488 (2008). [PubMed: 19029901]
3. Gorman GS et al. Prevalence of nuclear and mitochondrial DNA mutations related to adult mitochondrial disease. *Annals of Neurology* 77, 753–759 (2015). [PubMed: 25652200]
4. Srivastava S & Moraes CT Manipulating mitochondrial DNA heteroplasmy by a mitochondrially targeted restriction endonuclease. *Human molecular genetics* 10, 3093–3099 (2001). [PubMed: 11751691]
5. Tanaka M et al. Gene therapy for mitochondrial disease by delivering restriction endonuclease SmaI into mitochondria. *Journal of biomedical science* 9, 534–541 (2002). [PubMed: 12372991]
6. Stewart JB & Chinnery PF Extreme heterogeneity of human mitochondrial DNA from organelles to populations. *Nature Reviews Genetics* (2020).
7. Ahier A et al. Affinity purification of cell-specific mitochondria from whole animals resolves patterns of genetic mosaicism. *Nature cell biology* 20, 352–360 (2018). [PubMed: 29358705]
8. Chiang ACY, McCartney E, O'Farrell PH & Ma H A Genome-wide Screen Reveals that Reducing Mitochondrial DNA Polymerase Can Promote Elimination of Deleterious Mitochondrial Mutations. *Current Biology* 29, 4330–4336.e4333 (2019). [PubMed: 31786061]
9. Lin Y-F et al. Maintenance and propagation of a deleterious mitochondrial genome by the mitochondrial unfolded protein response. *Nature* 533, 416–419 (2016). [PubMed: 27135930]
10. Hahn A & Zuryn S The Cellular Mitochondrial Genome Landscape in Disease. *Trends Cell Biol* 29, 227–240 (2019). [PubMed: 30509558]
11. Pereira CV & Moraes CT Current strategies towards therapeutic manipulation of mtDNA heteroplasmy. *Front Biosci (Landmark Ed)* 22, 991–1010 (2017). [PubMed: 27814659]
12. Larsson NG & Clayton DA Molecular genetic aspects of human mitochondrial disorders. *Annu Rev Genet* 29, 151–178 (1995). [PubMed: 8825472]
13. Schon EA, DiMauro S, Hirano M & Gilkerson RW Therapeutic prospects for mitochondrial disease. *Trends Mol Med* 16, 268–276 (2010). [PubMed: 20556877]

14. Greaves LC et al. Clonal expansion of early to mid-life mitochondrial DNA point mutations drives mitochondrial dysfunction during human ageing. *PLoS genetics* 10, e1004620 (2014). [PubMed: 25232829]
15. Bender A et al. High levels of mitochondrial DNA deletions in substantia nigra neurons in aging and Parkinson disease. *Nature genetics* 38, 515–517 (2006). [PubMed: 16604074]
16. Gitschlag BL et al. Homeostatic responses regulate selfish mitochondrial genome dynamics in *C. elegans*. *Cell metabolism* 24, 91–103 (2016). [PubMed: 27411011]
17. Nargund AM, Fiorese CJ, Pellegrino MW, Deng P & Haynes CM Mitochondrial and nuclear accumulation of the transcription factor ATFS-1 promotes OXPHOS recovery during the UPR(mt). *Molecular cell* 58, 123–133 (2015). [PubMed: 25773600]
18. Shpilka T et al. UPRmt scales mitochondrial network expansion with protein synthesis via mitochondrial import in *Caenorhabditis elegans*. *Nature communications* 12 (2021).
19. Nargund AM, Pellegrino MW, Fiorese CJ, Baker BM & Haynes CM Mitochondrial Import Efficiency of ATFS-1 Regulates Mitochondrial UPR Activation. *Science* 337, 587–590 (2012). [PubMed: 22700657]
20. Bernstein SH et al. The mitochondrial ATP-dependent Lon protease: a novel target in lymphoma death mediated by the synthetic triterpenoid CDDO and its derivatives. *Blood* 119, 3321–3329 (2012). [PubMed: 22323447]
21. Tsang WY & Lemire BD Stable heteroplasmy but differential inheritance of a large mitochondrial DNA deletion in nematodes. *Biochem Cell Biol* 80, 645–654 (2002). [PubMed: 12440704]
22. Cristina D, Cary M, Lunceford A, Clarke C & Kenyon C A Regulated Response to Impaired Respiration Slows Behavioral Rates and Increases Lifespan in *Caenorhabditis elegans*. *PLoS genetics* 5, e1000450 (2009). [PubMed: 19360127]
23. Xu C et al. Genetic inhibition of an ATP synthase subunit extends lifespan in *C. elegans*. *Sci Rep* 8, 14836 (2018). [PubMed: 30287841]
24. Deng P et al. Mitochondrial UPR repression during *Pseudomonas aeruginosa* infection requires the bZIP protein ZIP-3. *Proceedings of the National Academy of Sciences* 116, 6146–6151 (2019).
25. Gustafsson CM, Falkenberg M & Larsson N-G Maintenance and Expression of Mammalian Mitochondrial DNA. *Annual review of biochemistry* 85, 133–160 (2016).
26. Rauthan M, Ranji P, Aguilera Pradenas N, Pítot C & Pilon M The mitochondrial unfolded protein response activator ATFS-1 protects cells from inhibition of the mevalonate pathway. *Proceedings of the National Academy of Sciences of the United States of America* 110, 5981–5986 (2013). [PubMed: 23530189]
27. Bota DA & Davies KJA Lon protease preferentially degrades oxidized mitochondrial aconitase by an ATP-stimulated mechanism. *Nature cell biology* 4, 674–680 (2002). [PubMed: 12198491]
28. Liu T et al. DNA and RNA binding by the mitochondrial lon protease is regulated by nucleotide and protein substrate. *The Journal of biological chemistry* 279, 13902–13910 (2004). [PubMed: 14739292]
29. Chen SH, Suzuki CK & Wu SH Thermodynamic characterization of specific interactions between the human Lon protease and G-quartet DNA. *Nucleic acids research* 36, 1273–1287 (2008). [PubMed: 18174225]
30. Matsushima Y, Goto YI & Kaguni LS Mitochondrial Lon protease regulates mitochondrial DNA copy number and transcription by selective degradation of mitochondrial transcription factor A (TFAM). *Proceedings of the National Academy of Sciences* 107, 18410–18415 (2010).
31. Göke A et al. Mrx6 regulates mitochondrial DNA copy number in *S. cerevisiae* by engaging the evolutionarily conserved Lon protease Pim1. *Molecular Biology of the Cell*, mbc.E19-08-0470 (2019).
32. Valenci I, Yonai L, Bar-Yaacov D, Mishmar D & Ben-Zvi A Parkin modulates heteroplasmy of truncated mtDNA in *Caenorhabditis elegans*. *Mitochondrion* 20, 64–70 (2015). [PubMed: 25462019]
33. Kukat C et al. Cross-strand binding of TFAM to a single mtDNA molecule forms the mitochondrial nucleoid. *Proc Natl Acad Sci U S A* 112, 11288–11293 (2015). [PubMed: 26305956]
34. King MP & Attardi G Human cells lacking mtDNA: repopulation with exogenous mitochondria by complementation. *Science* 246, 500–503 (1989). [PubMed: 2814477]

35. Bruno C et al. A stop-codon mutation in the human mtDNA cytochrome c oxidase I gene disrupts the functional structure of complex IV. *Am J Hum Genet* 65, 611–620 (1999). [PubMed: 10441567]
36. Moraes CT et al. Mitochondrial DNA deletions in progressive external ophthalmoplegia and Kearns-Sayre syndrome. *N Engl J Med* 320, 1293–1299 (1989). [PubMed: 2541333]
37. Moraes CT, Schon EA, DiMauro S & Miranda AF Heteroplasmy of mitochondrial genomes in clonal cultures from patients with Kearns-Sayre syndrome. *Biochem Biophys Res Commun* 160, 765–771 (1989). [PubMed: 2541710]
38. Yusoff AAM, Abdullah WSW, Khair S & Radzak SMA A comprehensive overview of mitochondrial DNA 4977-bp deletion in cancer studies. *Oncol Rev* 13, 409 (2019). [PubMed: 31044027]
39. Lee HC, Pang CY, Hsu HS & Wei YH Differential accumulations of 4,977 bp deletion in mitochondrial DNA of various tissues in human ageing. *Biochim Biophys Acta* 1226, 37–43 (1994). [PubMed: 8155737]
40. Munch C & Harper JW Mitochondrial unfolded protein response controls matrix pre-RNA processing and translation. *Nature* 534, 710–713 (2016). [PubMed: 27350246]
41. Gilkerson RW et al. Mitochondrial autophagy in cells with mtDNA mutations results from synergistic loss of transmembrane potential and mTORC1 inhibition. *Human molecular genetics* 21, 978–990 (2012). [PubMed: 22080835]
42. Paix A, Folkmann A, Rasoloson D & Seydoux G High Efficiency, Homology-Directed Genome Editing in *Caenorhabditis elegans* Using CRISPR-Cas9 Ribonucleoprotein Complexes. *Genetics* 201, 47–54 (2015). [PubMed: 26187122]
43. Mukhopadhyay A, Deplancke B, Walhout AJM & Tissenbaum HA Chromatin immunoprecipitation (ChIP) coupled to detection by quantitative real-time PCR to study transcription factor binding to DNA in *Caenorhabditis elegans*. *Nature protocols* 3, 698–709 (2008). [PubMed: 18388953]
44. Li H & Durbin R Fast and accurate short read alignment with Burrows-Wheeler transform. *Bioinformatics* 25, 1754–1760 (2009). [PubMed: 19451168]
45. Zhang Y et al. Model-based analysis of ChIP-Seq (MACS). *Genome Biol* 9, R137 (2008). [PubMed: 18798982]
46. Robinson JT et al. Integrative genomics viewer. *Nat Biotechnol* 29, 24–26 (2011). [PubMed: 21221095]
47. Blankenberg D et al. Manipulation of FASTQ data with Galaxy. *Bioinformatics* 26, 1783–1785 (2010). [PubMed: 20562416]
48. Zhang J, Kobert K, Flouri T & Stamatakis A PEAR: a fast and accurate Illumina Paired-End reAd mergeR. *Bioinformatics* 30, 614–620 (2014). [PubMed: 24142950]
49. Belmonte FR et al. Digital PCR methods improve detection sensitivity and measurement precision of low abundance mtDNA deletions. *Scientific Reports* 6, 25186 (2016). [PubMed: 27122135]
50. Fiorese CJ et al. The Transcription Factor ATF5 Mediates a Mammalian Mitochondrial UPR. *Curr Biol* 26, 2037–2043 (2016). [PubMed: 27426517]
51. Pham T-ND, Ma W, Miller D, Kazakova L & Benchimol S Erythropoietin inhibits chemotherapy-induced cell death and promotes a senescence-like state in leukemia cells. *Cell death & disease* 10, 22 (2019). [PubMed: 30622244]
52. Haynes CM, Yang Y, Blais SP, Neubert TA & Ron D The Matrix Peptide Exporter HAF-1 Signals a Mitochondrial UPR by Activating the Transcription Factor ZC376.7 in *C. elegans*. *Molecular cell* 37, 529–540 (2010). [PubMed: 20188671]
53. Palikaras K, Lionaki E & Tavernarakis N Coordination of mitophagy and mitochondrial biogenesis during ageing in *C. elegans*. *Nature* 521, 525–528 (2015). [PubMed: 25896323]
54. Fang EF et al. NAD⁺ augmentation restores mitophagy and limits accelerated aging in Werner syndrome. *Nature communications* 10 (2019).
55. Weiss KR, Voigt FF, Shepherd DP & Huisken J Tutorial: practical considerations for tissue clearing and imaging. *Nature protocols* 16, 2732–2748 (2021). [PubMed: 34021294]

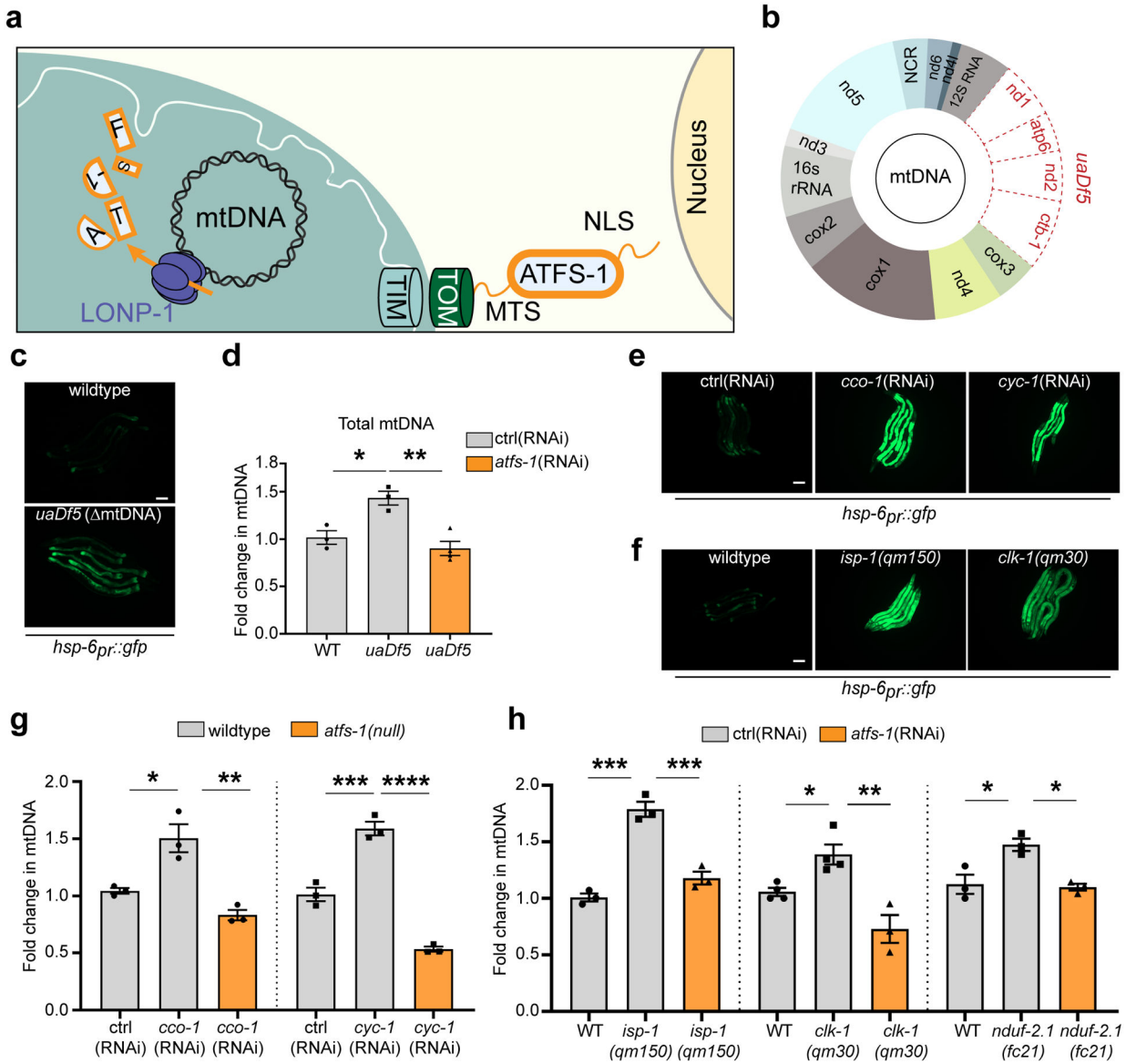


Fig. 1 | OXPHOS dysfunction increases mtDNAs through ATFS-1.

a, ATFS-1/UPR^{mt} signaling schematic in healthy cells. **b**, Comparison of wildtype and *uaDf5* deletion (*mtDNA*) mtDNAs. **c**, Photomicrographs of *hsp-6_{pr}::gfp* and *hsp-6_{pr}::gfp;uaDf5* worms (Scale bar 0.1 mm). Representative images from four biological repeats. **d**, Quantification of total mtDNA in homoplasmic wildtype, *uaDf5* worms and *uaDf5* worms raised on *atfs-1*(RNAi). *n* = 3, biologically independent samples. **P* = 0.0176, ***P* = 0.0034. **e**, Photomicrographs of *hsp-6_{pr}::gfp* worms raised on control (ctrl), *cco-1* or *cyc-1*(RNAi). Representative images from four biological repeats. **f**, Photomicrographs of wildtype, *isp-1(qm150)* and *clk-1(qm30);hsp-6_{pr}::gfp* worms. (Scale bar 0.1 mm). Representative images from four biological repeats. **g**, Quantification of total mtDNA in homoplasmic wildtype and *atfs-1*(null) worms raised on control(RNAi), *cco-1*(RNAi), or *cyc-1*(RNAi). *n* = 3, biologically independent samples. **P* = 0.0128, ***P* = 0.002, ****P* = 0.0005, *****P* < 0.0001. **h**, Quantification of mtDNA in wildtype,

isp-1(qm150), *clk-1(qm30)* or *nduf-2.1(fc21)* mutant worms raised on control(RNAi) or *atfs-1*(RNAi). $n = 3$ (WT, *isp-1(qm150)*, *isp-1(qm150) atfs-1*(RNAi)), biologically independent samples. *** $P = 0.0001$ and 0.0005 (WT vs. *isp-1(qm150)* and *isp-1(qm150) atfs-1*(RNAi)). $n = 4$ (WT, *clk-1(qm30)*), $n = 3$ (*clk-1(qm30) atfs-1*(RNAi)), biologically independent samples. * $P = 0.0443$, ** $P = 0.0016$ (WT, *clk-1(qm30)* and *clk-1(qm30) atfs-1*(RNAi)). $n = 3$ (WT, *nduf-2.1(fc21)* and *nduf-2.1(fc21) atfs-1*(RNAi)), biologically independent samples. * $P = 0.0151$ and 0.011 (WT vs. *nduf-2.1(fc21)* and *nduf-2.1(fc21) atfs-1*(RNAi)). Each biologically independent sample contained 40–60 animals and every dot stands for averaged value from 3 technical replicates in **d,g** and **h**; One-way ANOVA was used in **d,g** and **h**; data shown represent mean \pm S.E.M. * $P < 0.05$, ** $P < 0.01$, *** $P < 0.001$, **** $P < 0.0001$.

Author Manuscript

Author Manuscript

Author Manuscript

Author Manuscript

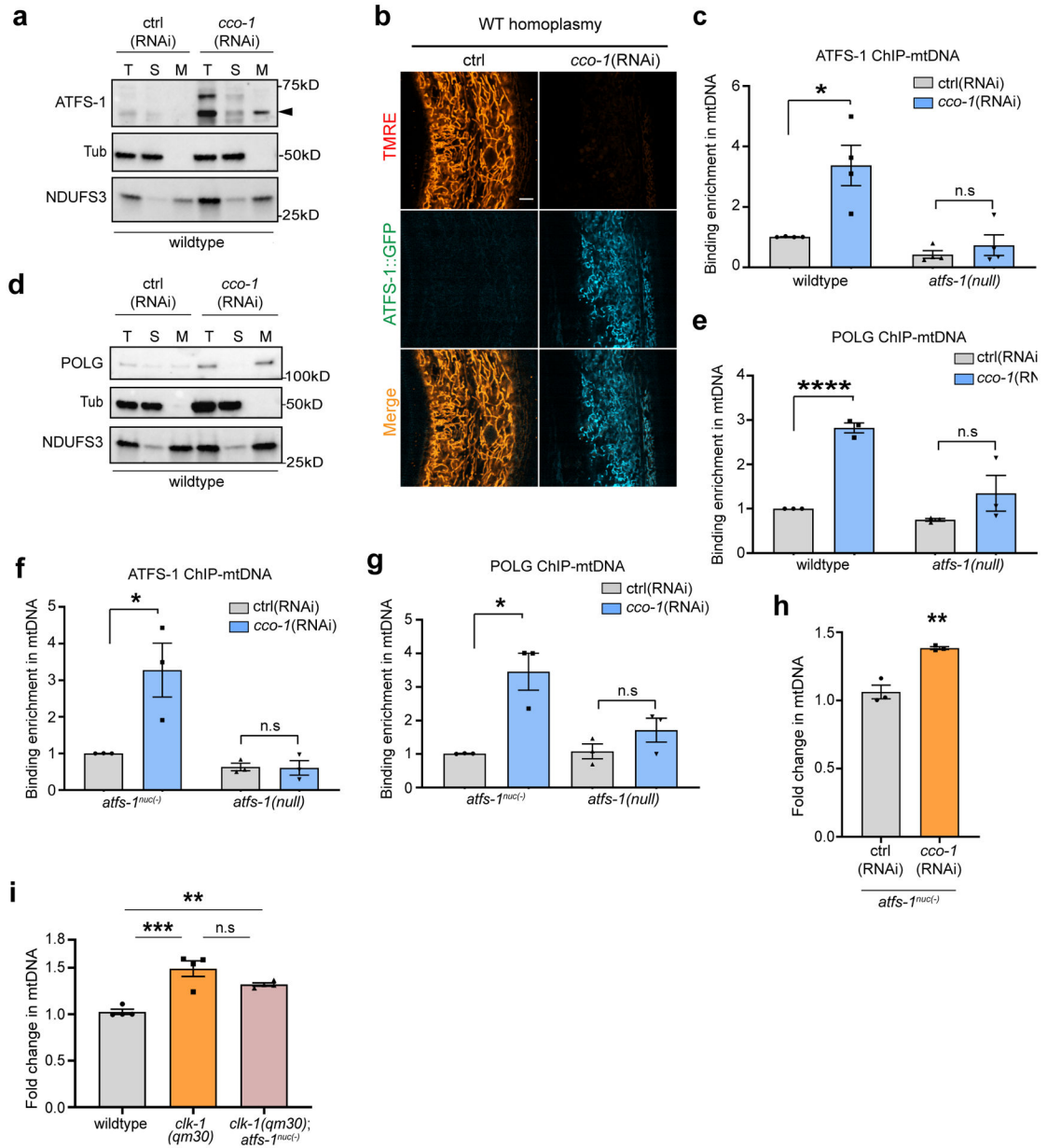


Fig. 2 | Defective OXPHOS impedes the degradation of ATFS-1 and facilitates mitochondrial-localized ATFS-1 and POLG binding to mtDNAs.

a, ATFS-1 immunoblots of wildtype worms raised on control or *cco-1*(RNAi) after fractionation into total lysate (T), post-mitochondrial supernatant (S), and mitochondrial pellet (M). Tubulin (Tub) and the OXPHOS component (NDUFS3) are used as loading controls. Arrow is mitochondrial-localized ATFS-1. Representative immunoblots from three biological repeats. **b**, *atfs-1_{pr}::atfs-1::gfp* transgenic animals raised on control(RNAi) or *cco-1*(RNAi) with TMRE staining (Scale bar 5µm). Representative images from three biological repeats. **c**, Quantification of mtDNA following ATFS-1 ChIP-mtDNA in homoplasmic wildtype worms and homoplasmic *atfs-1*(null) worms raised on control or *cco-1*(RNAi). *n* = 4, biologically independent samples. **P* = 0.0121. **d**, POLG immunoblots of wildtype worms raised on control or *cco-1*(RNAi) after mitochondrial fractionation.

Representative immunoblots from three biological repeats. **e**, Quantification of total mtDNA following POLG ChIP-mtDNA in wildtype or *atfs-1(null)* homoplasmic worms. $n = 3$, biologically independent samples. **** $P < 0.0001$. **f**, Quantification of mtDNA following ATFS-1 ChIP-mtDNA in homoplasmic *atfs-1^{nuc(-)}* worms and homoplasmic *atfs-1(null)* worms raised on control or *cco-1(RNAi)*. $n = 3$, biologically independent samples. * $P = 0.0363$. **g**, Quantification of total mtDNA following POLG ChIP-mtDNA in homoplasmic *atfs-1^{nuc(-)}* and *atfs-1(null)* worms raised on control or *cco-1(RNAi)*. $n = 3$, biologically independent samples. * $P = 0.0113$. **h**, Quantification of total mtDNA in *atfs-1^{nuc(-)}* homoplasmic worms raised on control(RNAi) or *cco-1(RNAi)*. $n = 3$, biologically independent samples. ** $P = 0.0033$. **i**, Quantification of total mtDNA in wildtype, *clk-1(qm30)* and *clk-1(qm30);atfs-1^{nuc(-)}* homoplasmic wildtype worms. $n = 4$, biologically independent samples. ** $P = 0.0081$, *** $P = 0.0004$, One-way ANOVA. Each biologically independent sample contained about 150,000 animals in **c,e-g**; contained 40–60 animals in **h,i**; every dot stands for averaged value from 3 technical replicates); Two-tailed Student's t test was used in **c** and **e-i**; data shown represent mean \pm S.E.M.

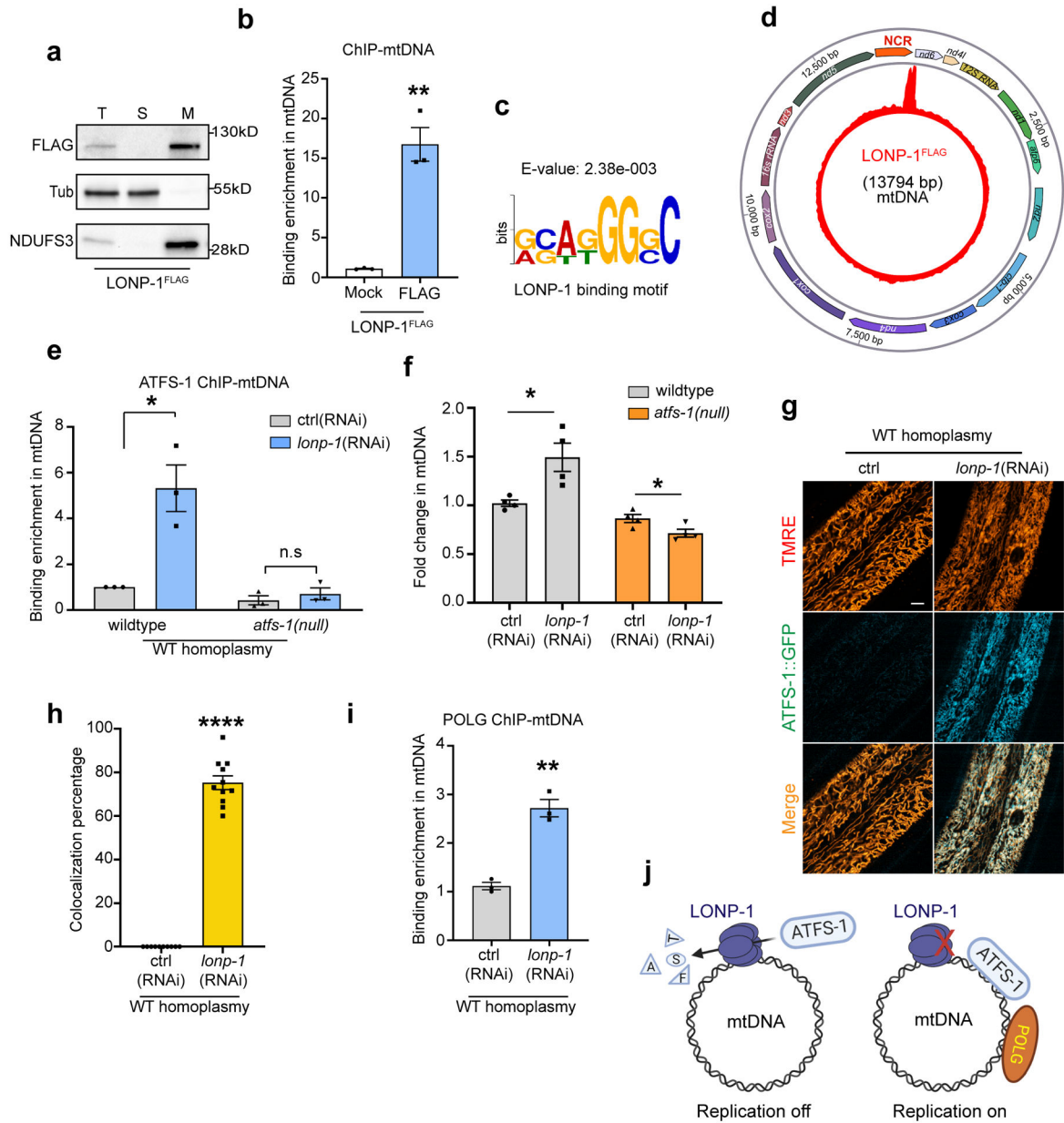


Fig. 3 | LONP-1 limits ATFS-1 binding to wildtype mtDNAs and impairs replication.

a, FLAG immunoblots of LONP-1^{FLAG} worms following fractionation into total lysate (T), post-mitochondrial supernatant (S), and mitochondrial pellet (M). Tubulin (Tub) and the OXPHOS component NDUFS3 are loading controls. Representative immunoblots from four biological repeats. **b**, Quantification of mtDNA from homoplasmic LONP-1^{FLAG} worms following ChIP-mtDNA using FLAG or control (Mock) antibody. $n = 3$, biologically independent samples. $**P = 0.0018$. **c**, LONP-1 consensus binding motif within mtDNA. **d**, ChIP-seq profile of mtDNA from homoplasmic LONP-1^{FLAG} worms raised on control(RNAi) using FLAG antibody (red). **e**, Quantification of total mtDNA following ATFS-1 ChIP-mtDNA in wildtype or *atfs-1(null)* homoplasmic worms raised on control(RNAi) or *lonp-1*(RNAi). $n = 3$, biologically independent samples. $*P = 0.0132$.

f, Quantification of mtDNA in homoplasmic wildtype and *atfs-1(null)* worms raised on control(RNAi) or *lonp-1*(RNAi). $n = 4$, biologically independent samples. $*P < 0.05$. **g-h**, *atfs-1_{pr}::atfs-1::gfp* transgenic animals raised on control(RNAi) or *lonp-1*(RNAi) with TMRE staining (Scale bar 5 μ m) (**g**); Percentage of mitochondria with co-localized TMRE and ATFS-1::GFP. $n = 10$ ctrl(RNAi) and $n = 11$ *lonp-1*(RNAi), biologically independent samples. $****P < 0.0001$ (**h**). **i**, Quantification of total mtDNA following POLG ChIP-mtDNA in wildtype homoplasmic worms raised on control(RNAi) or *lonp-1*(RNAi). $n = 3$, biologically independent samples. $**P = 0.0012$. **j**, Schematic of the relationship between LONP-1 activity, mitochondrial ATFS-1 accumulation and mtDNA replication. Each biologically independent sample contained about 150,000 worms in **b,e,i**; each sample contained 40–60 animals in **f**; every dot stands for averaged value from 3 technical replicates in **b,e,f** and **i**; Two-tailed Student's t test was used; data shown represent mean \pm S.E.M.

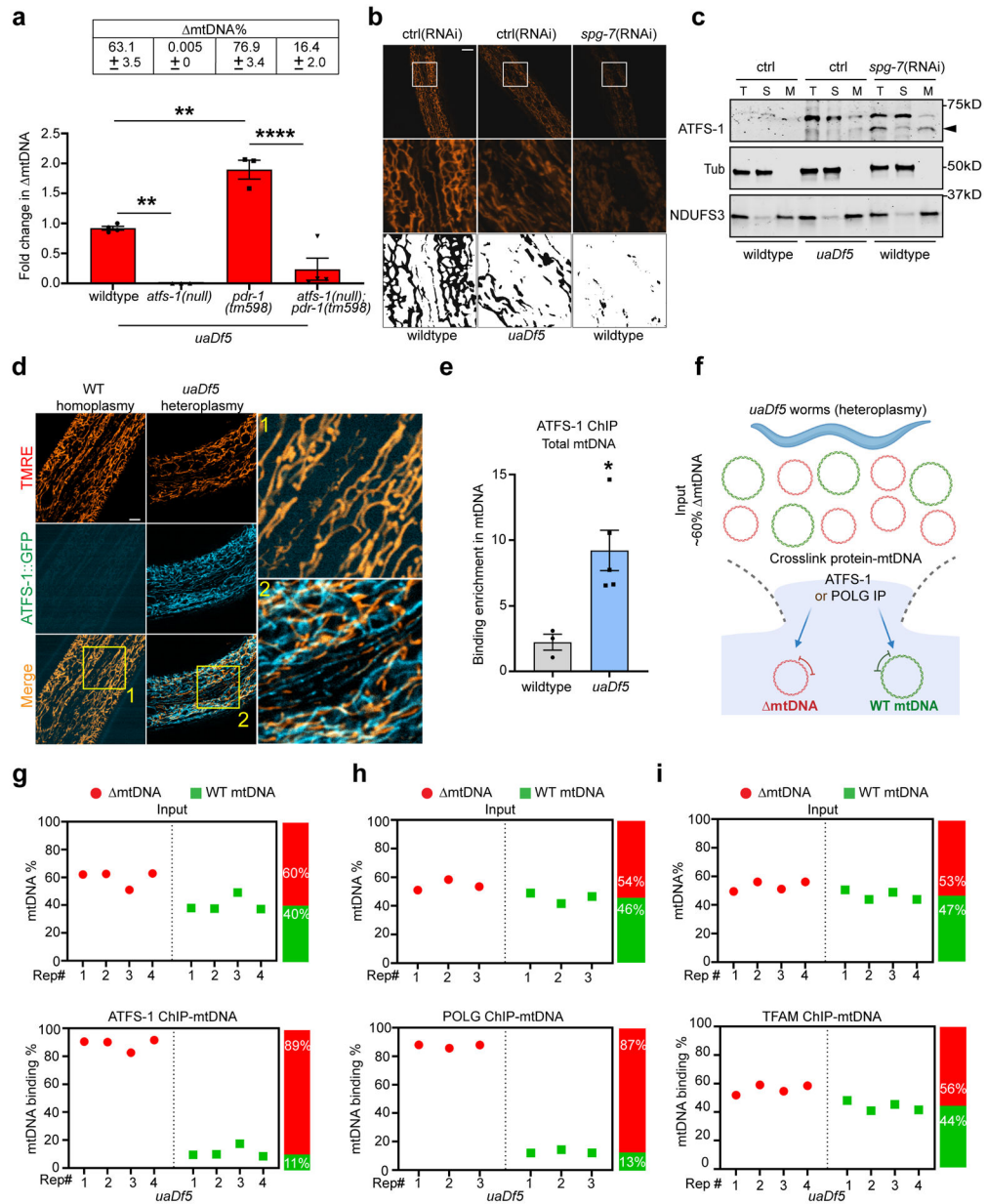


Fig. 4 | ATFS-1 and POLG primarily interact with mtDNAs in heteroplasmic worms.
a, mtDNA quantification as determined by qPCR in *uaDf5* worms, *atfs-1(null);uaDf5*, *pdr-1(tm598);uaDf5* and *atfs-1(null);pdr-1(tm598);uaDf5* worms. $n = 4$ (*uaDf5* and *atfs-1(null);pdr-1(tm598);uaDf5*) and $n = 3$ (*atfs-1(null);uaDf5* and *pdr-1(tm598);uaDf5*) biologically independent samples. ** $P < 0.01$ and **** $P < 0.0001$, One-way ANOVA.
b, Images of TMRE-stained micrographs of heteroplasmic (Δ mtDNA) worms raised on control(RNAi), or wildtype worms raised on control or *spg-7*(RNAi). Scale bar, 10 μ M. Representative images from four biological repeats. **c**, Immunoblots of wildtype worms raised on control or *spg-7*(RNAi) and heteroplasmic (Δ mtDNA) worms raised on control(RNAi) after fractionation into total lysate (T), post-mitochondrial supernatant (S), and mitochondrial pellet (M). Tubulin (Tub) and the OXPHOS component

(NDUFS3) are used as loading controls. Arrow is mitochondrial-localized ATFS-1. Representative immunoblots from three biological repeats. **d**, *atfs-1_{pr}::atfs-1::gfp* or *atfs-1_{pr}::atfs-1::gfp;uaDf5* transgenic animals with TMRE staining (Scale bar 5 μ m). Representative images from six biological repeats. **e**, Quantification of total mtDNA following ATFS-1 ChIP-mtDNA in homoplasmic wildtype or Δ mtDNA worms. $n = 3$ wildtype and $n = 5$ *uaDf5* biologically independent samples. * $P = 0.0226$, two-tailed Student's t test. **f**, Workflow of ATFS-1 or POLG ChIP-mtDNA and quantification of wildtype mtDNA and Δ mtDNA in heteroplasmic worms. **g**, Quantification of wildtype mtDNA and Δ mtDNA by qPCR following ATFS-1 ChIP-mtDNA in heteroplasmic worms. Post-lysis/Input Δ mtDNA ratio was 60%. $n = 4$, biologically independent samples. **h**, Quantification of wildtype mtDNA and Δ mtDNA by qPCR following POLG ChIP-mtDNA in heteroplasmic worms. Post-lysis/Input Δ mtDNA ratio was 54%. $n = 3$, biologically independent samples. **i**, Quantification of wildtype mtDNA and Δ mtDNA following TFAM IP-mtDNA in heteroplasmic worms. Post-lysis/Input Δ mtDNA ratio was 53%. $n = 4$, biologically independent samples. Each biologically independent sample contained 40–60 animals in **a**; each biologically independent sample contained about 150,000 worms in **e,g-i**; every dot stands for averaged value from 3 technical replicates in **a,e** and **g-i**; data shown represent mean \pm S.E.M.

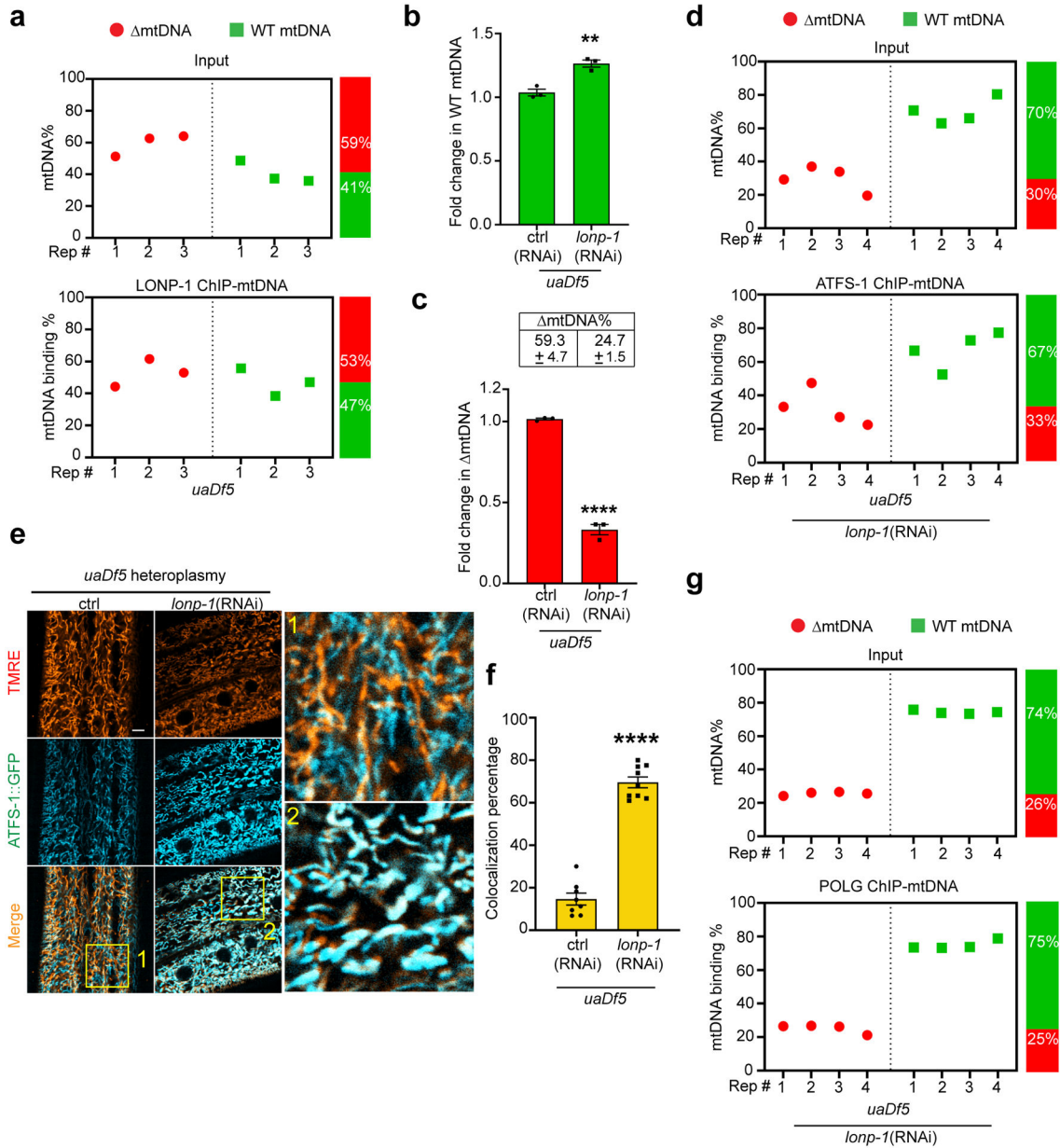


Fig. 5 | LONP-1 is required to maintain heteroplasmy.
a, mtDNA and wildtype mtDNA quantification by qPCR following LONP-1 ChIP-mtDNA in heteroplasmic worms. Post-lysis/Input mtDNA ratio was 59%. $n = 3$, biologically independent samples. **b**, Quantification of wildtype mtDNA by qPCR in heteroplasmic worms raised on control(RNAi) or *lonp-1*(RNAi). $n = 3$, biologically independent samples. ** $P = 0.0041$. **c**, Quantification of ΔmtDNA by qPCR in heteroplasmic *uaDf5* worms raised on control(RNAi) or *lonp-1*(RNAi). $n = 3$, biologically independent samples. **** $P < 0.0001$. **d**, mtDNA and wild-type mtDNA quantification by qPCR following ATFS-1 ChIP-mtDNA in heteroplasmic worms raised on control(RNAi) or *lonp-1*(RNAi). $n = 4$, biologically independent samples. **e-f**, *atfs-1_{pr}::atfs-1::gfp;uaDf5* transgenic animals raised on control(RNAi) or *lonp-1*(RNAi) with TMRE staining (Scale bar 5μm) (**e**); Percentage

of mitochondria with co-localized TMRE and ATFS-1::GFP. $n = 8$ *uaDf5* ctrl(RNAi) and $n = 9$ *uaDf5 lonp-1*(RNAi), biologically independent samples (**f**). **g**, mtDNA and wild-type mtDNA quantification by qPCR following POLG ChIP-mtDNA in heteroplasmic worms raised on *lonp-1*(RNAi). Post-lysis/Input mtDNA ratio was 25%. $n = 4$, biologically independent samples. Each biologically independent sample contained about 150,000 animals in **a,d,g**; each biological replicate contained 40–60 animals in **b,c**; every dot stands for averaged value from 3 technical replicates in **a-d and g**; Two-tailed Student's t test was used in **b,c and f**; data shown represent mean \pm S.E.M.

Author Manuscript

Author Manuscript

Author Manuscript

Author Manuscript

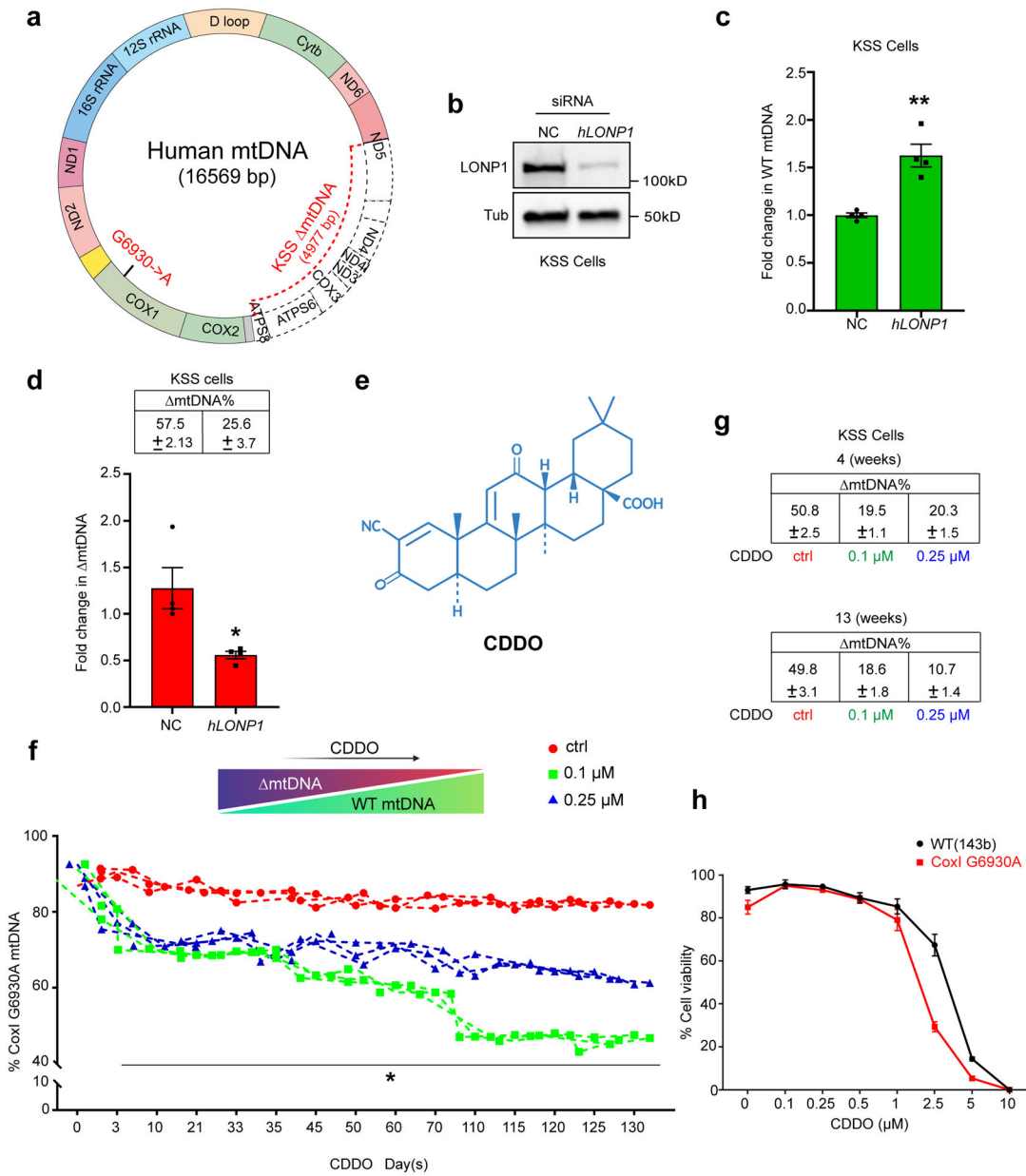


Fig. 6 | LONP1 inhibition improves heteroplasmy in cybrid cells.

a, Schematic comparing human wildtype, KSS deletion (Δ mtDNA) and CoxI G6930A mtDNAs. **b**, LONP1 immunoblots from KSS heteroplasmic cells treated with *hLONP1* or control (NC) siRNA. Tubulin (Tub) serves as a loading control. Representative immunoblots from three biological repeats. **c**, WT mtDNA quantification in KSS cells treated with control or *hLONP1* siRNA. $n = 4$, biologically independent samples. $**P = 0.0021$. **d**, Quantification of KSS Δ mtDNA in cells treated with control or *hLONP1* siRNA. $n = 4$, biologically independent samples. $*P = 0.0185$. **e**, Chemical structure of CDDO. **f**, Quantification of G6930A mtDNA percentage following treatment with DMSO, 0.1 μ M CDDO, or 0.25 μ M CDDO at the indicated time points up to 130 days. $n = 3$, biologically independent samples. $*P < 0.05$. **g**, Δ mtDNA quantification in KSS heteroplasmic cells

treated with DMSO, 0.1 μ M CDDO, or 0.25 μ M for 4 or 13 weeks. **h**, Cell viability of 143b (WT) and CoxI G6930A cells exposed to the indicated concentration of CDDO for 72 hours. $n = 3$ in 143b(WT) cell or CoxI G6930A cell, biologically independent samples. Every dot stands for averaged value from 3 technical replicates in **c,d**; Two-tailed Student's t test was used in **c,d** and **f**; data shown in **c**, **d** and **h** represent mean \pm S.E.M.

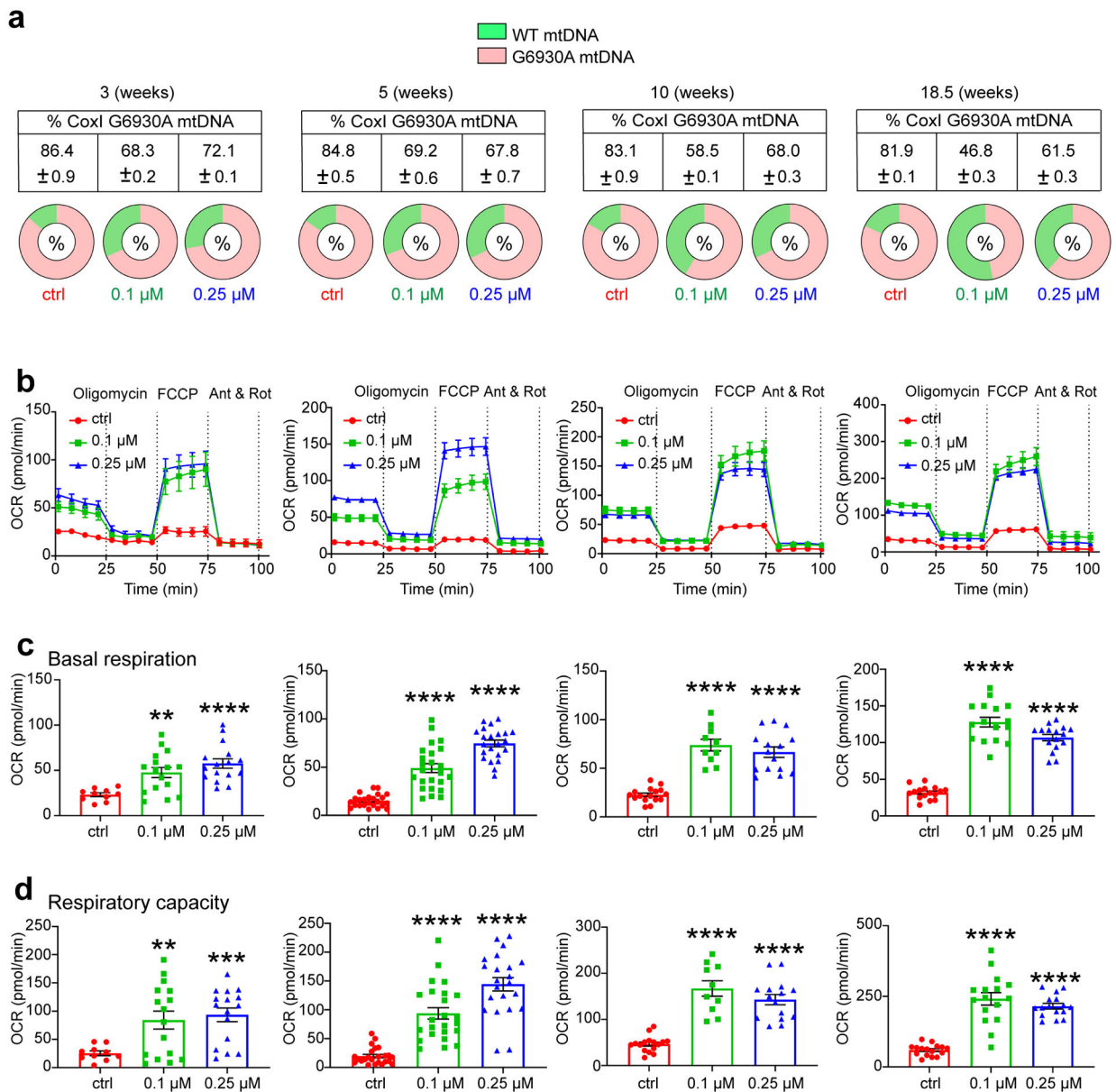


Fig. 7 |. Pharmacological inhibition of LONP1 improves heteroplasmy and OXPHOS function in cybrid cells.

a, Percentage of CoxI G6930A mtDNA in cells treated with DMSO, 0.1 μM or 0.25 μM CDDO for 3, 5, 10 or 18.5 weeks. $n = 3$, biologically independent samples. These data are extracted from Fig. 6f. **b**, Oxygen consumption rates (OCR) of CoxI G6930A cells treated with DMSO, 0.1 μM or 0.25 μM CDDO for 3, 5, 10 or 18.5 weeks. **c**, Quantification of basal respiration. In 3 weeks, $n = 10$ (ctrl), $n = 16$ (0.1 μM) and $n = 16$ (0.25 μM), biologically independent samples. $**P = 0.0028$, $****P < 0.0001$. In 5 weeks, $n = 24$ (ctrl), $n = 24$ (0.1 μM) and $n = 22$ (0.25 μM), biologically independent samples. $****P < 0.0001$. In 10 weeks, $n = 16$ (ctrl), $n = 10$ (0.1 μM) and $n = 15$ (0.25 μM), biologically independent samples. $****P < 0.0001$. In 18.5 weeks, $n = 16$ (ctrl, 0.1 μM and 0.25 μM), biologically independent samples. $****P < 0.0001$. **d**, Quantification of respiratory capacity. In 3 weeks, $n = 10$ (ctrl),

$n = 16$ (0.1 μM) and $n = 16$ (0.25 μM), biologically independent samples. $**P = 0.0086$, $***P = 0.0002$. In 5 weeks, $n = 24$ (ctrl), $n = 24$ (0.1 μM) and $n = 22$ (0.25 μM), biologically independent samples. $****P < 0.0001$. In 10 weeks, $n = 16$ (ctrl), $n = 10$ (0.1 μM) and $n = 15$ (0.25 μM), biologically independent samples. $****P < 0.0001$. In 18.5 weeks, $n = 16$ (ctrl, 0.1 μM and 0.25 μM), biologically independent samples. $****P < 0.0001$. Every dot stands for averaged value from 4 technical replicates in **c,d**; Two-tailed Student's t test was used in **c,d**; data shown in **b-d** represent mean \pm S.E.M..